



HAL
open science

Pentacoordinated, Square-Pyramidal Cationic PCP Ni(II) Pincer Complexes: ELF and QTAIM Topological Analyses of Nickel-Triflate Interactions Graphical abstract

Christine Lepetit, Boris Vabre, Yves Canac, Mohammad Esmail Alikhani,
Davit Zargarian

► **To cite this version:**

Christine Lepetit, Boris Vabre, Yves Canac, Mohammad Esmail Alikhani, Davit Zargarian. Pentacoordinated, Square-Pyramidal Cationic PCP Ni(II) Pincer Complexes: ELF and QTAIM Topological Analyses of Nickel-Triflate Interactions Graphical abstract. *Theoretical Chemistry Accounts: Theory, Computation, and Modeling*, 2018, 137 (11), pp.141. hal-01950168

HAL Id: hal-01950168

<https://hal.sorbonne-universite.fr/hal-01950168v1>

Submitted on 10 Dec 2018

HAL is a multi-disciplinary open access archive for the deposit and dissemination of scientific research documents, whether they are published or not. The documents may come from teaching and research institutions in France or abroad, or from public or private research centers.

L'archive ouverte pluridisciplinaire **HAL**, est destinée au dépôt et à la diffusion de documents scientifiques de niveau recherche, publiés ou non, émanant des établissements d'enseignement et de recherche français ou étrangers, des laboratoires publics ou privés.

Pentacoordinated, Square-Pyramidal Cationic PCP Ni(II) Pincer Complexes: ELF and QTAIM Topological Analyses of Nickel-Triflate Interactions

Christine Lepetit,^{*a} Boris Vabre,^b Yves Canac,^{*a} Mohammad Esmail Alikhani,^{*c} and
Davit Zargarian^{*b}

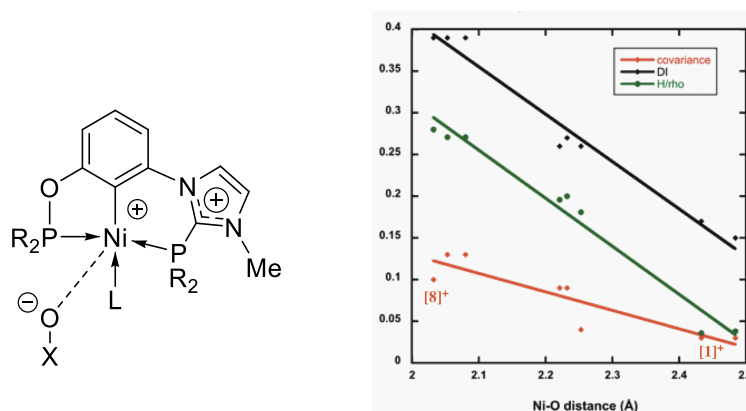
[a] LCC-CNRS, Université de Toulouse, CNRS, Toulouse, France.

[b] Département de Chimie, Université de Montréal, Montréal, Québec H3C 3J7, Canada.

[c] Sorbonne Universités, UPMC Université Paris 06, MONARIS, UMR 8233, Université Pierre et Marie Curie, 4 Place Jussieu, Case courrier 49, F-75252 Paris Cedex 05, France.

E-mail: christine.lepetit@lcc-toulouse.fr, yves.canac@lcc-toulouse.fr, esmail.alikhani@sorbonne-universite.fr, zargarian.davit@umontreal.ca

Graphical abstract



The cationic charge of the pincer ligand induces a weakly covalent ionic Ni-O interaction with the counter-anion OX. Measurements using QTAIM (DI, H/ρ , Eint) and absolute values of ELF covariances $|\langle \bar{\sigma}^2(V(O), C(Ni)) \rangle|$ have allowed us to estimate the covalence degree of the Ni-O interaction as a function of anion OX, *P*-substituents R, and co-ligands L.

Abstract: A previous report introduced a new series of cationic nickel(II) complexes ligated by PCP-type pincer ligands featuring a charge-bearing imidazoliophosphine binding moiety, and described their catalytic reactivities in hydroamination of nitriles into amidines. Solid state characterization of the cationic acetonitrile adducts $[(R\text{-PIMIOCOP}^+)\text{Ni}(\text{NCMe})(\text{triflate})]^+$ ($R\text{-PIMIOCOP}^+ = \kappa^P, \kappa^C, \kappa^P\text{-}\{2\text{-(R}_2\text{PO)}, 6\text{-(R}_2\text{PC}_4\text{H}_5\text{N}_2)\text{C}_6\text{H}_3\}$; $R = i\text{-Pr}$, **[1]**⁺; Ph, **[2]**⁺) carried out in this follow-up study showed a distorted square-pyramidal geometry and a Ni-triflate distance that was shorter than the sum of the Ni and O van der Waals radii, features suggestive of an unusual pentacoordination at the Ni(II) center. In contrast, the related aquo adduct $[(i\text{-Pr-PIMIOCOP}^+)\text{Ni}(\text{OH}_2)(\text{triflate})]^+$, **[3]**⁺, displayed a more conventional square planar geometry. Detailed structural comparisons and theoretical analyses conducted on these and related compounds have allowed a thorough examination of the Ni-triflate interactions in this family of complexes. Thus, topological analysis of the Electron Localization Function (ELF) and Quantum Theory of Atoms In Molecules (QTAIM) showed that the Ni-triflate interaction is mostly ionic in nature, but has a weak covalence degree. The monosynaptic $V(\text{Ni})$ subvalence basin of nickel is indeed the ELF signature of the covalence degree of the ionic Ni-O bond, which can be quantified by the negative QTAIM energy density at the Ni-O bond critical point and by the absolute value of the ELF covariance $\langle \sigma^2(V(\text{O}), C(\text{Ni})) \rangle$. The ionic character of the Ni-O bond is also reflected in an Energy Decomposition Analysis (EDA), showing that this interaction is mostly electrostatic in nature. The computational analyses carried out on this family of complexes provide valuable insight into the character and relative strengths of various Ni-ligand interactions, and allow a number of useful conclusions, including the following: (i) significant Ni-anion interactions at the apical site are observed only with pincer-type ligands featuring at least one cationic imidazoliophosphine binding moiety; (ii) these primarily electrostatic Ni-O interactions gain increasing covalence degree when different pincer backbone, co-ligand L, or counter-anion are introduced to enhance the electron deficiency of the Ni(II) center.

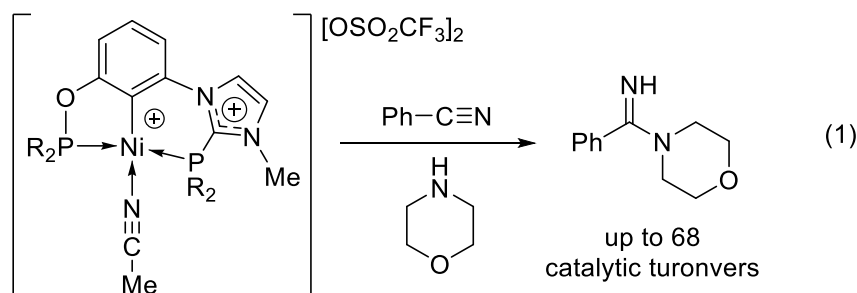
Keywords: Pentacoordination, pincer, ELF, QTAIM, EDA, subvalence ELF basins, covalence degree, ionic bonding, imidazoliophosphine.

Introduction

Organometallic complexes of d^8 ions bearing one or more strong-field ligands such as CO, olefins, and hydrocarbyl fragments R constitute a distinct class of compounds that frequently disobey the “18-electron rule” by forming tetracoordinate, 16-electron compounds that are thermally stable and adopt low-spin square planar coordination geometry. Indeed, this phenomenon is so general as to have prompted some researchers to invoke a “16-electron rule” and a “square-planar paradigm” for organometallic complexes of d^8 ions,¹ in particular for Rh(I), Ir(I), Pd(II), Pt(II) and Au(III). Of course, there are also many thermally stable pentacoordinate compounds that are in violation to this “16-electron rule” by virtue of being (at least nominally) 18-electron species; this is especially true for the 3d ions Co(I) and Ni(II).

In this class of pentacoordinate organometallic complexes, those bearing ligands that can participate in fundamental organometallic reactivities such as migratory insertion, oxidative addition and reductive elimination are particularly interesting, because they can serve as models for the proposed transition states of these reactions. A previous review has catalogued and analyzed various structural and electronic aspects of pentacoordinate organometallic complexes of d^8 ions that belong in this category.² An important structural feature of many of these compounds is the presence of at least one unusually long (and presumably weak) metal-ligand bond, often observed for the apical ligand in a square planar geometry.³ In cases wherein a bond distance in such pentacoordinate complexes approaches or surpasses the sum of covalent radii, it becomes important to have criteria other than experimentally obtained distances for establishing the degree and character of the metal-ligand interactions in question. We have encountered just such an example, which is the subject of this report.

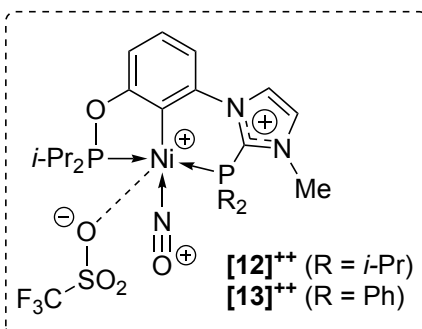
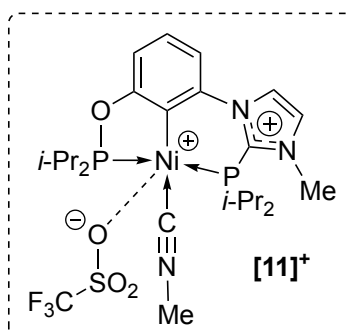
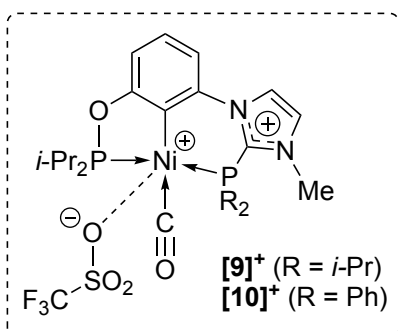
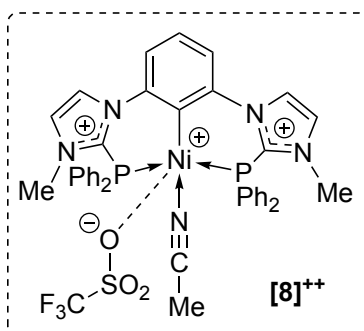
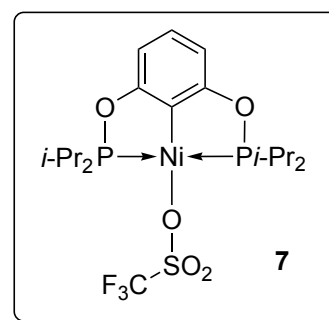
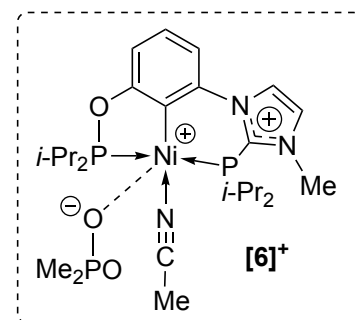
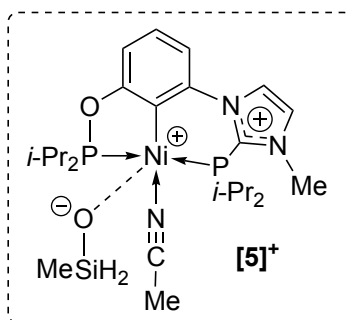
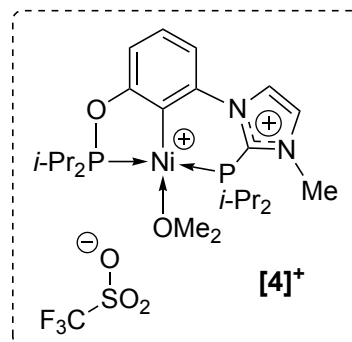
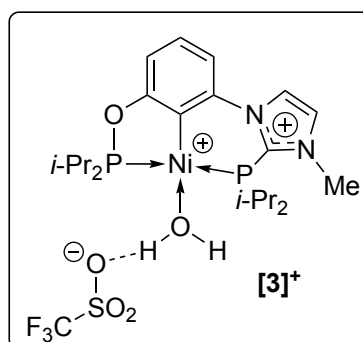
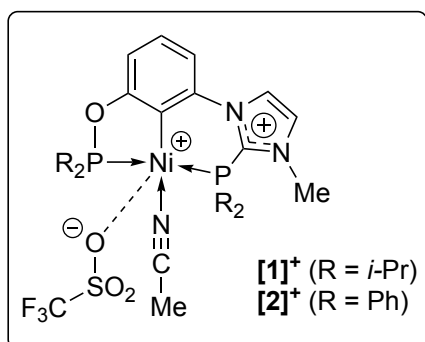
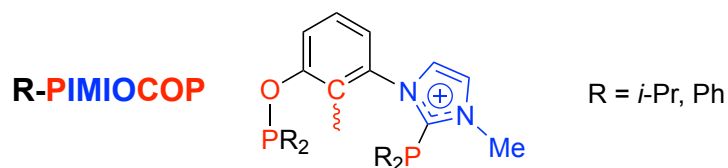
During the course of our investigations into the development of thermally stable yet fairly reactive pincer-type complexes of Ni(II), we reported a new family of compounds based on PCP-type PIMCOP and PIMIOCOP pincer ligands featuring both electron-rich and electron-poor donor extremities.⁴ Some of these complexes proved to be efficient pre-catalysts for the hydroamination of nitriles into amidines (eq. 1).



To complement our mechanistic studies of the above catalytic process, we set out to isolate and structurally characterize various derivatives (mono- and dicationic) of these complexes. This effort led to the expected tetracoordinate, square planar complexes,^{4b} but we also came across the pentacoordinated cations **[1]**⁺ and **[2]**⁺ (Chart 1) that were unanticipated. The experimental solid state structures of these complexes revealed a square-pyramidal geometry wherein the Ni-triflate_(apical) distance was unusually long, but still lower than the sum of the corresponding van der Waals radii. The true character of the Ni-triflate interactions in these complexes was rendered more ambiguous due to the fact that these normally weakly coordinating anionic ligands might also be influenced by the positive charge borne by the imidazolium moiety of the pincer ligand. It should be noted that the incidence of pentacoordination with phenylene-based pincer complexes of divalent Ni is quite uncommon: to the best of our knowledge, the closely related pincer complexes (PSiP)Ni(PMe₃)X (PSiP = κ^3 -(2-Ph₂PC₆H₄)₂SiMe; X = Cl, Br, I)⁵ are the only examples of this category of compounds.⁶

The above considerations prompted us to launch a theoretical study to determine whether the Ni-triflate interactions found in **[1]**⁺ and **[2]**⁺ constitute a conventional covalent bond. This report presents the experimental structures of these compounds and results of systematic theoretical analyses undertaken to characterize the Ni-OTf (OTf = triflate anion, OSO₂CF₃) and other Ni-ligand interactions. We have applied Molecular Orbital (MO) analysis, Energy Decomposition Analysis (EDA), Electron Localization Function (ELF) and Quantum Theory of Atoms in Molecules (QTAIM) topological analyses on **[1]**⁺ and **[2]**⁺ as well as a number of closely related compounds—real and hypothetical—derived by varying the main components of the compounds, i.e., the pincer ligand, the co-ligand, and the anion itself (Chart 1). These analyses have allowed us to determine the influence of these variables on the character of the Ni-anion interactions, indicating that the latter can be modulated by judicious choice of the various components of the complexes. The combined results of these analyses have indicated that the Ni-triflate interactions observed in the title pentacoordinate complexes are best described as ionic interactions with a weak covalence degree.

Chart 1. Line drawings of the various complexes studied. Compounds bordered in solid rectangles have been synthesized, characterized spectroscopically and by single crystal X-ray diffraction studies, whereas those in dashed rectangles are hypothetical compounds studied by computational analyses only.



Results and Discussion

I. Ni-OTf interaction in PIMIOCOP pincer-type Ni complexes

I-1. Synthesis and characterization of PIMIOCOP complexes [1-3]⁺. The cationic acetonitrile adducts [1]⁺ and [2]⁺ were prepared by addition of silver triflate to the previously reported bromo precursors, as shown in Scheme 1. The synthesis and spectroscopic characterization of these cationic compounds has been reported elsewhere,^{4b} whereas their solid state characterization by single crystal X-ray diffraction studies was undertaken in the course of the present study. Suitable single crystals of [1]⁺ and [2]⁺ were grown for this purpose from their saturated chloroform solutions kept at -37 °C. Single crystals of the analogous aquo adduct [3]⁺ were obtained when [1]⁺ was recrystallized in wet THF at -37 °C, presumably because the coordinated acetonitrile in this compound was displaced by the residual solvent moisture. The molecular structures of these compounds are shown in Figure 1 along with the most relevant solid state parameters; the structures are described below.

Scheme 1. Synthesis of the cationic acetonitrile and aquo adducts [1-3]⁺.

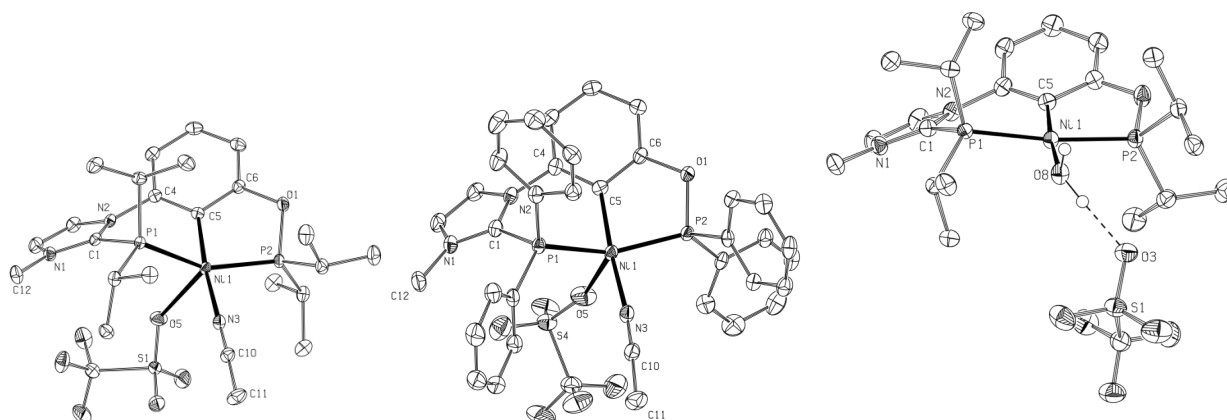
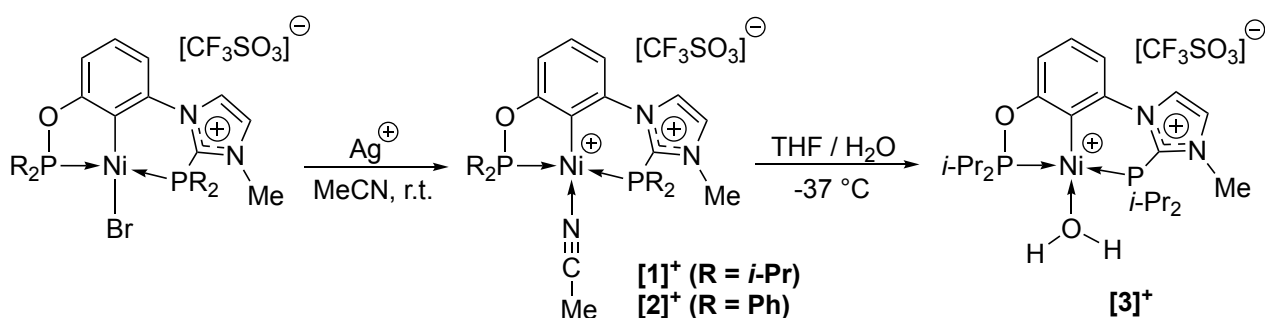


Figure 1. ORTEP diagrams of Ni(II) complexes [1]⁺ (*left*), [2]⁺ (*middle*), and [3]⁺ (*right*). Thermal ellipsoids are shown at the 50% probability level. Hydrogen atoms and second triflate anion have been omitted for clarity. Bond lengths (Å) and angles (°): Ni-C5 = 1.914(2) ([1]⁺), 1.929(2) ([2]⁺), 1.922(2) ([3]⁺); Ni-N3/O8 = 1.893(2) ([1]⁺), 1.890(2) ([2]⁺), 1.940(2) ([3]⁺); Ni-P1 2.224(1) ([1]⁺),

2.2104(8) ([2]⁺), 2.227(1) ([3]⁺); Ni-P2 = 2.153(1) ([1]⁺), 2.1492(7) ([2]⁺), 2.169(1) ([3]⁺); Ni-O5 = 2.433(2) ([1]⁺), 2.350(2) ([2]⁺); P1-Ni-P2 = 152.53(2) ([1]⁺), 153.53(3) ([2]⁺), 173.36(3) ([3]⁺); C5-Ni-N3/O8 = 174.50 ([1]⁺), 174.96 ([2]⁺), 174.70 ([3]⁺); P1-Ni-O5 = 92.53 ([1]⁺), 97.44 ([2]⁺); P2-Ni-O5 = 112.55 ([1]⁺), 107.92 ([2]⁺). P1-Ni-C5 = 94.36 ([3]⁺); P1-Ni-O8 = 88.96 ([3]⁺); P2-Ni-C5 = 83.52 ([3]⁺); P2-Ni-O8 = 92.73 ([3]⁺).

The Ni center in [3]⁺ adopts a square-planar geometry, as would be anticipated for a d⁸ ion coordinated by strong-field P- and C- based ligands. In contrast, the Ni centers in the two acetonitrile adducts [1]⁺ and [2]⁺ appear to adopt a pentacoordinated geometry as a result of a close contact between the Ni center and the oxygen atom of the triflate anion. The most obvious hint of pentacoordination is the observed Ni-OTf distances of 2.433 Å ([1]⁺) and 2.350 Å ([2]⁺), which are longer than the sum of corresponding covalent (1.90 Å) and ionic radii (1.95 Å), but much shorter than the sum of the van der Waals radii of Ni and O atoms (3.15 Å). For comparison, the Ni-O distance in the aquo adduct [3]⁺ is 1.94 Å.

Other indications of pentacoordination in [1]⁺ and [2]⁺ include major tetragonal distortions arising from the Ni-OTf interaction. For instance, whereas the “trans” P-Ni-P angles are *ca.* 173° in the aquo adduct, the corresponding angle in the acetonitrile adducts is *ca.* 153°. The Ni centers in the latter are also significantly out of the main square plane of the ligands compared to [3]⁺,⁷ by *ca.* 0.27 Å in [1]⁺, 0.25 Å in [2]⁺, and only *ca.* 0.09 Å in [3]⁺. These considerations suggest that the Ni-OTf interactions exert significant influence on the solid state structures of the acetonitrile adducts [1]⁺ and [2]⁺, and the τ index of 0.36 derived for these compounds points to a distorted square pyramidal geometry.⁸

The apparent pentacoordination observed in [1]⁺ and [2]⁺ was unexpected, because most pincer Ni(II) complexes reported to date display variously distorted square planar geometries of the type found in the aquo adduct [3]⁺.⁹ Close inspection of the solid state structure of the latter compound revealed that the oxygen atom of the triflate anion interacts with an hydrogen atom of the coordinated H₂O molecule instead of the Ni center, the HOH---OTf distance being 1.709 Å. Such a hydrogen bonding interaction between Ni-OH₂ and OTf anion has been observed previously.¹⁰ The unusual pentacoordination in the solid-state structures of the acetonitrile adducts [1]⁺ and [2]⁺ prompted us to use complementary theoretical tools to investigate the nature of Ni-OTf interactions at the apical site, as described in the following sections.

I-2. Calculated structures of [1-3]⁺ and related isomers. The structures of [1]⁺, [2]⁺, and [3]⁺ were calculated at the PCM-B3PW91/6-31G** level with implicit acetonitrile solvent as a dielectric continuum. Figures 2 and 3 show the structures resulting from this approach side by side with the

corresponding experimentally derived structures; comparison of main structural parameters showed good pair-wise agreement between these structures. We also computed a structural isomer of $[1]^+$ in which the relative positions of NCMe and the triflate anion were exchanged; this structure turned out to be less stable by 8.4 kcal/mol compared to $[1]^+$ (Figure S1 in SI).

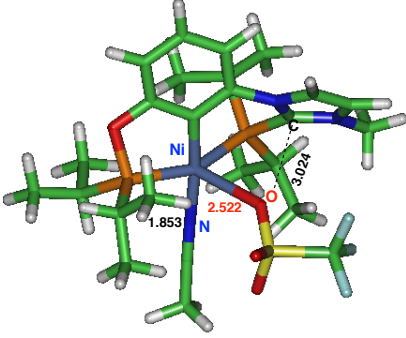
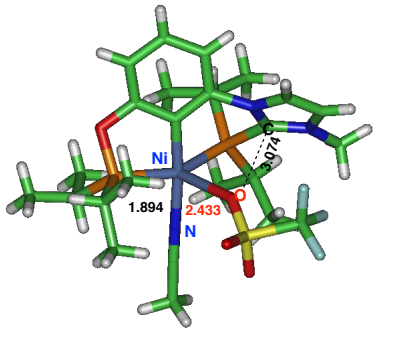
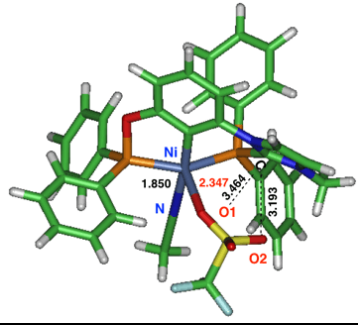
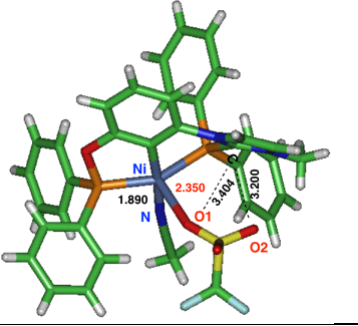
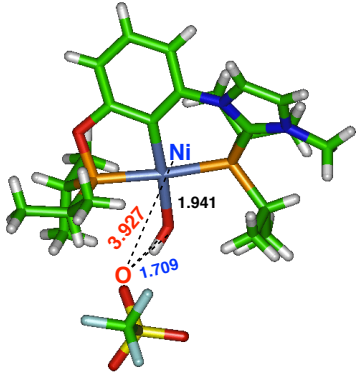
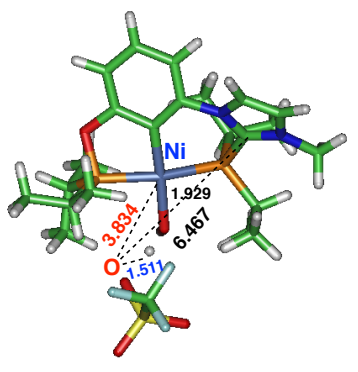
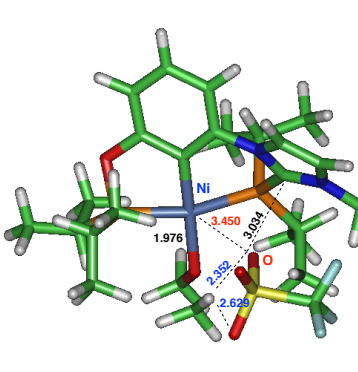
	
[1]⁺ (calc.) Ni-O: 2.522 Å and N ₂ C-OTf: 3.024 Å Ni-N(CCH ₃): 1.853 Å	[1]⁺ (exp.) Ni-O: 2.433 Å and N ₂ C-OTf: 3.074 Å Ni-N(CCH ₃): 1.894 Å
	
[2]⁺ (calc.) Ni-O1: 2.347 Å and N ₂ C-O2Tf: 3.193 Å Ni-N(CCH ₃): 1.850 Å and N ₂ C-O1Tf: 3.464	[2]⁺ (exp.) Ni-O1: 2.350 Å and N ₂ C-O2Tf: 3.200 Å Ni-N(CCH ₃): 1.890 Å and N ₂ C-O1Tf: 3.404 Å

Figure 2. Selected geometrical data for calculated (*left*) and experimentally determined (*right*) structures for complexes $[1]^+$ (*top*) and $[2]^+$ (*bottom*).

		
[3]⁺ (exp.) Ni-OTf: 3.927 Å N ₂ C-OTf: 6.647 Å Ni _{5c} -O(H) ₂ : 1.941 Å	[3]⁺ (calc.) Ni-OTf: 3.834 Å N ₂ C-OTf: 6.467 Å Ni-O(H) ₂ : 1.929 Å	[4]⁺ (calc.) Ni-OTf: 3.450 Å N ₂ C-OTf: 3.034 Å Ni-O(Me) ₂ : 1.976 Å

Hydrogen bond: 1.709 Å	Hydrogen bond: 1.511 Å	No hydrogen bonding
------------------------	------------------------	---------------------

Figure 3. Selected geometrical data for the experimental structure of complex **[3]⁺** (*left*) and the structures calculated at the PCM-B3PW91/6-31G** level in acetonitrile solvent for **[3]⁺** (*middle*) and the related OMe₂ adduct **[4]⁺** (*right*).

The structure computed for the aquo adduct **[3]⁺**, which was also quite comparable to the experimentally derived structure, showed that substitution of NCMe by water led to loss of the Ni-OTf interaction in favor of a new hydrogen bonding interaction between the triflate anion and the aquo ligand (Figure 3 and Figure S2). To determine if the loss of Ni-OTf interaction in **[3]⁺** is due entirely to the presence of the protic sites in the aquo ligand, we computed the structure of the OMe₂ adduct **[4]⁺**, a new cationic adduct in which the aquo protons are replaced by methyl groups. The results of this study revealed that the Ni-OTf distance did shorten as a result of replacing the aquo ligand by OMe₂ (from 3.834 Å calc. for **[3]⁺** to 3.450 Å calc. for **[4]⁺**), but a significant interaction of the type observed in **[1]⁺** and **[2]⁺** is not re-established as judged by the rather long Ni-O distance. Instead, the triflate anion in **[4]⁺** interacts with the imidazolium ring (N₂C-OTf = 3.034 Å). These results suggest that the bulkiness of the methyl groups may prevent the Ni-OTf interaction, resulting in a closer contact with the next nearest positively charged moiety, namely the imidazolium ring. In the space filling model of **[4]⁺** shown in Figure S3, the Van der Waals spheres of Ni and O are indeed not overlapping. Hydrogen bonding with the OMe₂ group and non-covalent interactions similar to those observed in complex **1** between the oxygen atom of the triflate and the imidazolium ring are expected (see QTAIM section II.2). These observations seemed to imply that the interactions of the triflate anion are mainly governed by electrostatic factors. This conclusion was also supported by the results of calculations showing that rotational isomers of **[1]⁺** featuring various orientations of the triflate anion with respect to the cationic pincer backbone are iso-energetic with respect to **[1]⁺**, their relative energies being within 3.0 kcal/mol (Figures S1 and S2).

All the above results, namely a flat potential energy surface with quasi-degenerate conformers, various iso-energetic orientations of OTf and absence of any MO overlap related to a covalent interaction, suggest an ionic Ni-OTf bond. The nature of this bond was further investigated using topological analyses, as described hereafter.

e^- versus $4.42 e^-$ for $V(C,N)$) and within the accepted range of ELF populations accuracy (few percent using the default ELF analysis setup).¹² It is also noted that the topological descriptions and the aromatic character of the phenylene ring in both species are fairly insensitive to the incorporation of the triflate anion in the calculations. Thus, we conclude that the global topological descriptions of these species are very similar, which in turn implies that the Ni-OTf interactions must be of a primarily closed-shell ionic character.

A closer look at the ELF descriptions of complexes **[1]**⁺ and **[2]**⁺ (Figure 4) shows that the first coordination sphere of the Ni center is defined by a core Ni basin, $C(Ni)$, surrounded by the following five valence basins: two monosynaptic basins, $V(Ni)$ and $V(N)$, and three disynaptic basins related to the bonds with the two P-based ligands and the central phenylene ring, *i.e.*, $V(Ni,PO)$, $V(Ni,PIm)$ and $V(Ni,C)$. The QTAIM atomic contributions of Ni to these basin populations are sizeable (Table 1): $V(Ni,C)$ (16%), $V(Ni,PIm)$ (15%) and $V(Ni,PO)$ (*ca.* 20%). Significantly, the $V(Ni,C)$ attractor is located at about one third of the Ni-C bond closer to C; similarly, the $V(Ni,PIm)$ attractor is at about one third of the Ni-P bond closer to P. These features, along with the large covariance of these disynaptic basins with $C(Ni)$ (approx. -0.40), are consistent with the presence of $C \rightarrow Ni$ and $P \rightarrow Ni$ dative bonds in complexes **[1]**⁺ and **[2]**⁺; the same topological description of the first coordination sphere of the Ni center holds for complex **[3]**⁺ (Table 1).

The much lower QTAIM atomic contribution of Ni to $V(N)$ (4.4 %) and the smaller covariance with $C(Ni)$ ($\langle \bar{\sigma}^2(V(N), C(Ni)) \rangle = -0.22$) are indicative of a weaker donor-acceptor character for the $CH_3CN \rightarrow Ni$ interaction relative to the $C \rightarrow Ni$ and $P \rightarrow Ni$ bonds. In complex **[3]**⁺, only one of the two monosynaptic $V(O)$ basins is involved in the $H_2O \rightarrow Ni$ dative interaction. The small QTAIM atomic contribution of Ni (3.6 %) to this monosynaptic basin and the small covariance $\langle \bar{\sigma}^2(V(O), C(Ni)) \rangle = -0.08$ (Table 1) suggest that the $H_2O \rightarrow Ni$ dative bond in complex **[3]**⁺ is even weaker than the corresponding $CH_3CN \rightarrow Ni$ interaction in pincer complexes **[1]**⁺ and **[2]**⁺. Although the atomic charge of Ni in complexes **[1-3]**⁺ is only about 0.6 (Figure 4), the formal oxidation state of the nickel atom estimated from ELF analysis is found close to +II. This is calculated by subtracting the total population of $C(Ni)$ and $V(Ni)$ given in Table S1, from the atomic number of nickel, namely: $28 - (25.79 + 0.29)$.¹³

Table 1. ELF analysis of the dative Ni-X bonds (X = C, PIm or PO, N or O) of complexes [1-3]⁺ in their experimental geometry.

	Ni-phenylene			Ni-PR ₂ (im) and Ni-PR ₂ (O)			Ni-NCMe or Ni-OH ₂		
	V(Ni,C) ^a	%Ni ^b	Cov. ^c	V(Ni,PO) ^a V(Ni,PIm) ^a	%Ni ^b	Cov. ^c	V(N _{CH₃CN}) ^a V(O _{H₂O}) ^a	%Ni ^b	Cov. ^d
[1] ⁺	2.14	16%	-0.36	2.15	20 %	-0.38	3.18	4.4 %	-0.22
				2.15	15 %	-0.30			
[2] ⁺	2.15	16%	-0.35	2.13	19 %	-0.38	3.19	4.4 %	-0.22
				2.11	15 %	-0.30			
[3] ⁺	2.28	17%	-0.33	2.08	19 %	-0.29	1.93	3.6 %	-0.08
				2.01	15 %	-0.22	2.32	0.4 %	-0.03

^a: Average population \bar{N} of the ELF valence basin (in e^-) ^b: QTAIM atomic contribution of Ni. ^c: covariance $\langle \bar{\sigma}^2(V(\text{Ni},X), C(\text{Ni})) \rangle$. ^d: covariance $\langle \bar{\sigma}^2(V(X), C(\text{Ni})) \rangle$. B3PW91/6-31G** level of calculation.

Having established the ELF parameters for the main in-plane Ni-ligand bonds, we turn our attention to the out-of-plane Ni-OTf interactions in complexes [1-2]⁺. Recall that a covalent, electron-shared Ni-X bond should be *a priori* characterized by the presence of a V(Ni,X) disynaptic basin. That the Ni-OTf interaction in these complexes is not a covalent electron-shared bond, is indicated by the results of the ELF analysis showing no disynaptic basin, only two monosynaptic V(O) basins (Figure 4). Both of these V(O) basins exhibit negligible QTAIM atomic contributions from Ni (< 2 %) and negligible covariances with C(Ni) (< -0.03, Table 2), suggesting an ionic closed-shell interaction between Ni and OTf.

Additional indications that the Ni-OTf interaction in complex [1]⁺ is predominantly ionic in character are provided by the presence of a monosynaptic basin V(Ni) of low ELF value (0.311), low population (0.29 e^-), and large covariance with C(Ni) ($\langle \bar{\sigma}^2(V(\text{Ni}), C(\text{Ni})) \rangle = -0.17$). (See Table S2 in SI).¹⁴ Such subvalence basins V(M) resulting from the splitting of the outer-shell density of nickel have been shown by de Courcy *et al.* to be the topological signature of metal cations featuring an ionic interaction in biochemical systems.¹⁵ The volume and the population of the monosynaptic basins V(M) were reported to be sensitive to polarization effects and to increase with the covalence degree of the ionic bond.¹⁵

Notwithstanding the fairly similar ELF topological descriptions of [1]⁺ and [2]⁺ (Figure 4, Tables 1 and 2), the Ni-OTf interaction is anticipated to be slightly stronger in [2]⁺, because this complex displays a larger V(Ni) population (0.34 *vs* 0.29) and a greater covariance $\langle \bar{\sigma}^2(V(\text{Ni}), C(\text{Ni})) \rangle$ (-0.20 *vs* -0.17). This result is in accord with the less nucleophilic diphenylphosphine moiety, which would be expected to increase the electrophilicity of the Ni center in complex [2]⁺. On the other hand, the large population of V(Ni) in [3]⁺ is not related to the covalence degree of the Ni-OTf interaction but rather to that of the dative H₂O→Ni bond. Nevertheless, the ELF topological

description of the hydrogen bonding between the triflate anion and H₂O in [3]⁺ resembles the ELF topological description of the Ni-OTf interaction in complexes [1]⁺ and [2]⁺, suggesting a non-covalent interaction in all cases (Table 2).

Table 2. ELF analysis of the Ni-OTf interactions in the experimental geometry of [1-3]⁺.

OTf	V(O) ^a	%Ni ^b	Cov. ^c	V(O) ^a	%Ni ^b	Cov. ^c	V(Ni) ^a	ELF	Cov. ^d
[1] ⁺	2.64	0.02	-0.03	3.43	0.01	-0.03	0.29	0.311	-0.17
[2] ⁺	2.33	0.02	-0.03	3.76	0.01	-0.03	0.34	0.313	-0.20
[3] ⁺	2.17	0.00	-0.00	3.87	0.00	-0.00	1.58 ^e	0.261 ^e	-1.04 ^e

^a: Average population of the ELF valence basin (in e^-) ^b: QTAIM atomic contribution of Ni (in e^-). ^c: covariance $\langle \bar{\sigma}^2(V(O), C(Ni)) \rangle$. ^d: covariance $\langle \bar{\sigma}^2(V(Ni), C(Ni)) \rangle$. B3PW91/6-31G** level of calculation. ^e Highest accuracy level for ELF analysis (Grid = 0.05 Å and no cutoff for the gradient field analysis).

II-2. QTAIM topological analysis. The electronic structure of complex [1]⁺ and the bonding interactions in this compound were further studied using various QTAIM descriptors. The delocalization index (DI) quantifies the degree of covalence and the multiplicity of a given bond, and bonds may be classified according to the values of local indicators of electron density and energy densities calculated at the bond critical points (BCPs) (Table 3, Figure 5).¹⁶

Table 3. QTAIM descriptors (in a.u.) of selected bond critical points (BCP) involving the nickel atom or the oxygen atom of the triflate anion interacting with nickel in [1]⁺.^a

#BCP	BCP	ρ_{bcp}	$\Delta\rho_{\text{bcp}}$	V_{bcp} ^b	H_{bcp} ^c	$ H_{\text{bcp}} /\rho_{\text{bcp}}$	$ V_{\text{bcp}} /G_{\text{bcp}}$	DI ^d	E_{int} (kcal/mol)
10	Ni-C	0.1265	+0.192	-0.17779	-0.06492	0.51	1.58	0.82	55.8
42	Ni-PO	0.1094	+0.077	-0.14283	-0.06174	0.56	1.76	0.76	44.8
57	Ni-PI _m	0.0910	+0.106	-0.11857	-0.04607	0.51	1.64	0.66	37.2
19	Ni-NC	0.1008	+0.559	-0.18889	-0.02462	0.24	1.15	0.57	59.3
82	O-Ni	0.0284	+0.118	-0.03182	-0.00117	0.04	1.04	0.17	10.0
87	O---H	0.0039	+0.016	-0.00218	+0.00070	0.23	0.70	0.01	0.70
4	O---N	0.0088	+0.030	-0.00615	+0.00092	0.08	0.90	0.04	1.90

^a: See BCP location and labelling in Figure 6. ^b: Potential energy density V_{bcp} . ^c: Energy density H_{bcp} . ^d: Delocalization Index (DI). B3PW91/6-31G** level of calculation.

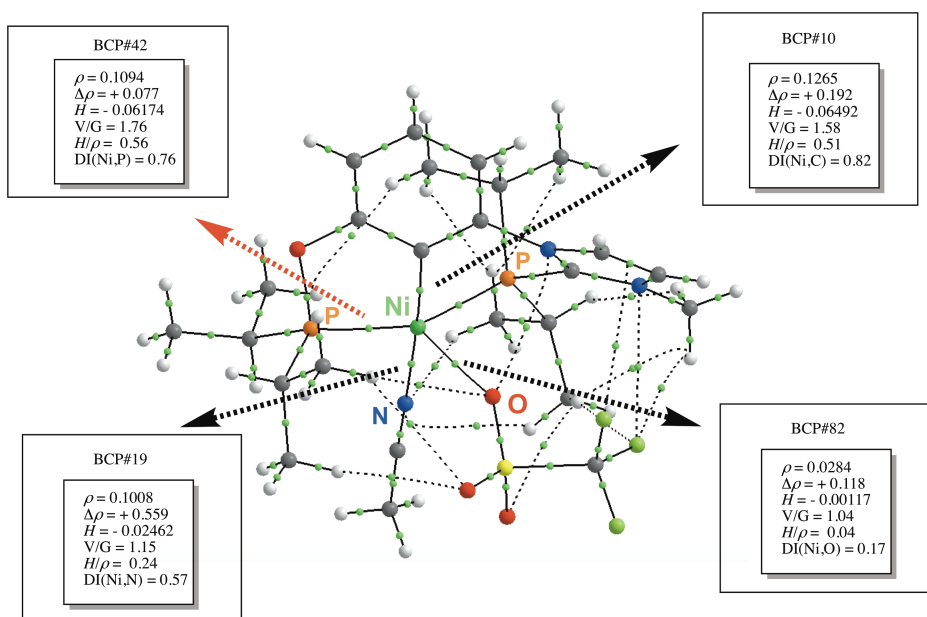


Figure 5. QTAIM molecular graph calculated at the B3PW91/6-31G** level for the experimental structure of complex $[1]^+$. Bond critical points are located as small green spheres. See main text and Table 3 for the definition of BCP descriptors.

Negative and positive values for the Laplacian of the electron density at the BCP ($\Delta\rho_{\text{bcp}}$) are assigned to « electron-shared » and « closed-shell » interactions, respectively.¹⁶ This classification was refined by Bianchi *et al.*¹⁷ into three bonding regimes, depending on the value of $|V_{\text{bcp}}|/G_{\text{bcp}}$, the ratio of the potential energy density V_{bcp} to the kinetic energy density G_{bcp} , as follows: a ratio greater than 2 is related to the shared-shell region of covalent bonds, while a smaller than one ratio is related to the closed-shell region of ionic bonds and van der Waals interactions; the intermediate region, $1 < |V_{\text{bcp}}|/G_{\text{bcp}} < 2$, includes dative bonds and ionic bonds of weak covalence degree.^{17,18}

Based on the above criteria and on Macchi's recent classification,¹⁹ the BCP descriptors related to the four Ni-ligand bonds in the main coordination plane are consistent with the presence of dative Ni←ligand bonds (Table 3, Figure 5).²⁰ For all these bonds, the $|V_{\text{bcp}}|/G_{\text{bcp}}$ ratio refers to the intermediate bond regime ($1 < |V_{\text{bcp}}|/G_{\text{bcp}} < 2$) according to the above-described classification of Bianchi *et al.*¹⁷ It should be added that these L→Ni bonds exhibit low electron density values ($0.09 < \rho_{\text{bcp}} < 0.13$ a.u.) and large positive Laplacian values $\Delta\rho_{\text{bcp}}$, ranging from +0.077 a.u. for the Ni-PO bond up to +0.559 for the Ni-NCCH₃ bond (Table 3). These parameters are also common to ionic bonds, but the latter display positive energy densities at the BCP (H_{bcp}), whereas these are negative in the present L→Ni interactions (Table 3).

According to Espinosa *et al.*,²¹ the “bond degree” $|H_{\text{bcp}}|/\rho_{\text{bcp}}$ may be useful for assigning the degree of covalence for any pairwise interaction. In complexes $[1-3]^+$, the bond degree is similar for the Ni-PIm, Ni-PO and Ni-C bonds ($|H_{\text{bcp}}|/\rho_{\text{bcp}} \approx 0.50$), while that for the Ni-NCCH₃ bond is half as

strong ($H_{\text{bcp}}/|\rho_{\text{bcp}}| = 0.24$), suggesting a larger ionic character in the latter case. The delocalization index (DI) values inferior to 1 are consistent with Ni-ligand bonds featuring a donor-acceptor character (Table 3), and suggest the following order for the increasing covalence degree of Ni-X bonds: Ni-N (DI = 0.57) < Ni-PIm (DI = 0.66) < Ni-PO (DI = 0.76) < Ni-C (DI = 0.82). It is noteworthy that the QTAIM Ni-ligand interaction energy estimated through Espinosa's correlation²² does not correlate with the covalence degree, as the Ni-NCCH₃ interaction is slightly stronger than the Ni-C interaction involving the central phenylene ring (Table 4). The QTAIM covalence degree and bond strength of the Ni←NCCH₃ dative bond is very similar in complexes [1]⁺ and [2]⁺ (Table 4). However, both the covalence degree (0.14 vs 0.24) and bond strength (47 vs 60 kcal/mol) of the Ni←OH₂ bond in [3]⁺ are significantly weaker (Table 4).

Table 4. QTAIM characteristics (in a.u.) of selected bond critical points (BCP) involving the nickel atom.^a

	BCP	DI	H_{bcp}	$ H_{\text{bcp}} / \rho_{\text{bcp}} $	E_{int} (kcal/mol)
[1] ⁺	Ni-NC	0.57	-0.02462	0.24	59.3
[2] ⁺	Ni-NC	0.57	-0.02472	0.24	60.0
[3] ⁺	Ni-OH ₂	0.46	-0.01135	0.14	46.6

^a See main text for the definition of BCP descriptors. B3PW91/6-31G** level of calculation.

Table 5 lists the QTAIM descriptions for (i) the Ni-OTf interaction in complexes [1]⁺ and [2]⁺ and (ii) the HOH-OTf interaction in complex [3]⁺. The two types of triflate interactions found in these complexes are of a similar character and strength (about 10 kcal/mol), as discussed below in the case of complex [1]⁺.

Table 5. QTAIM characteristics (in a.u.) of selected bond critical points (BCP) involving one oxygen atom of the triflate anion.^a

	BCP	DI	H_{bcp}	$ H_{\text{bcp}} / \rho_{\text{bcp}} $	$ V_{\text{bcp}} / G_{\text{bcp}} $	E_{int} (kcal/mol)
[1] ⁺	Ni-OTf	0.17	-0.00117	0.04	1.04	10.0
[2] ⁺	Ni-OTf	0.19	-0.00219	0.07	1.06	12.6
[3] ⁺	HOH-OTf	0.10	-0.00001	0.0002	1.00	10.1

^a: see main text for the definition of BCP descriptors. B3PW91/6-31G** level of calculation.

For the Ni-OTf interactions in [1]⁺, the values of $|V_{\text{bcp}}|/|G_{\text{bcp}}|$ are close to 1 (Table S4), that is to say they are at the boundary of the closed-shell region of ionic bonds and of the intermediate region ($1 < |V_{\text{bcp}}|/|G_{\text{bcp}}| < 2$), including dative and ionic bonds of weak covalence degree. The large positive value for the Laplacian of the electron density ($\Delta\rho_{\text{bcp}} = +0.118$ a.u.) and the low electron

density value (0.0284 a.u.) at the Ni-O BCP are indicative of an ionic, closed-shell type Ni-OTf interaction (Tables S3 and S4). A weak covalence degree is, nevertheless, anticipated from the sizeable value of the delocalization index (DI = 0.17, Table 5) and from the negative energy density value ($H_{\text{bcp}} = -0.001167$ a.u.). Both the degree of covalency, as measured by the $|H_{\text{bcp}}|/\rho_{\text{bcp}}$ ratio (0.04 a.u.), and the QTAIM Ni-O interaction energy of 10.0 kcal/mol, estimated from the Espinosa correlation,²² are non-negligible and also indicative of a weak covalence degree of the Ni-OTf ionic bond.

In the case of complex $[1]^+$, two weak non-bonding interactions of the triflate oxygen atom with one nitrogen atom of the imidazolium ring and with the hydrogen atom of the *i*-Pr substituent of the phosphinite moiety are also characterized by the related BCPs (Table 3). The positioning of the triflate anion results both from steric effects and the competition between three types of non-bonding interactions, namely TfO⁻--Ni⁺, TfO⁻--N₂C⁺, and TfO⁻--(CH₃)₂CH interactions (Figure 5 and Table 3).

II-3. Energy decomposition analysis (EDA). EDA allows for partitioning of the interaction energy between two fragments (E_{int}) into three components, namely: (i) the Pauli repulsion (E_{Pauli}); (ii) the electrostatic interactions (E_{elstat}) between the fragments frozen in the experimentally determined geometry of the complex; (iii) the orbital interaction energies (E_{orb}).²³ The latter accounts for charge transfer, which is related to interactions between occupied and empty orbitals of the metal fragment and the ligand, and for polarization effects corresponding to the mixing of orbitals within a given fragment. The Energy Decomposition Analysis will first be applied to Ni-OTf interactions in complexes $[1]^+$ and $[2]^+$, and to the Ni(OH₂)-OTf interaction in $[3]^+$, followed by the Ni-NCCH₃ interaction in $[1]^+$ and the Ni-OH₂ interaction in $[3]^+$.

The importance of E_{elstat} may be addressed in terms of its contribution to the total attractive interactions ($E_{\text{attr}} = E_{\text{elstat}} + E_{\text{orb}}$). The $E_{\text{elstat}} / E_{\text{attr}}$ is greater than 80% for the triflate interactions involved in complexes $[1-3]^+$ (Table 6). While it is true that E_{elstat} is significantly larger than E_{orb} , the underlying forces for E_{elstat} and E_{orb} are different in origin and their absolute values cannot be put on an equal footing. The ratio $E_{\text{int}} / E_{\text{elstat}}$, which places the total bond energy in relation to the electrostatic component, is therefore expected to provide a clearer bonding picture, such that the larger this ratio, the larger the influence of E_{elstat} on the chemical bond.²⁴ The $E_{\text{int}} / E_{\text{elstat}}$ ratio is larger than 90% for the triflate interactions involved in the series of complexes $[1-3]^+$ (Table 6), thus attributing a major electrostatic component to the Ni-OTf interaction. The $E_{\text{Pauli}} + E_{\text{orb}}$ sum may be related to an overall orbital contribution, *i.e.*, the result of destabilizing and stabilizing orbital overlaps. The ($E_{\text{Pauli}} + E_{\text{orb}}$) values are close to zero for the triflate interactions, consistent with an ionic Ni-OTf interaction (Table 6).

Table 6. EDA analyses of complexes **[1-3]⁺**. PBE/TZP level of calculation.

	Ni – OTf (Å)	E_{int}	E_{Pauli}	E_{elstat}	E_{orb}	$\frac{E_{\text{elstat}}}{E_{\text{attr}}}$	$\frac{E_{\text{int}}}{E_{\text{elstat}}}$	$\frac{E_{\text{Pauli}}}{E_{\text{orb}}}$
[1]⁺ (Ni --- OTf) ^a	2.433	-130.5	26.97	-135.28	-22.19	0.86	0.96	4.78
[2]⁺ (Ni --- OTf)	2.350	-129.98	34.80	-134.96	-29.83	0.82	0.96	4.97
[3]⁺ (NiOH ₂ --- OTf) ^a	1.511	-132.70	18.33	-125.90	-25.13	0.83	1.05	-6,80
[1]⁺ (Ni – NCCH ₃)	-	-47.51	80.46	-79.29	-48.68	0.62	0.60	31.78
[3]⁺ (Ni – OH ₂) ^a	-	-22.84	66.38	-59.34	-29.88	0.67	0.38	36.50

^a Energies (kcal/mol) calculated at the PBE/TZP level for the experimental geometries.

The EDA description of the CH₃CN→Ni and H₂O→Ni dative bonds is markedly different from that of the ionic Ni-OTf interactions in that smaller electrostatic contributions are found for CH₃CN→Ni (60%) and H₂O→Ni (38%). The Pauli and electrostatic contributions for these bonds nearly cancel each other, such that E_{int} is comparable to the orbital interaction energy contribution. As expected, the CH₃CN→Ni dative interaction is stronger than that of H₂O→Ni (47.5 vs 22.8 kcal/mol).

III. Modulation of the covalence degree of the ionic Ni-OTf bond

The above-presented EDA and topological (QTAIM and ELF) analyses point out that the Ni-OTf interaction in **[1]⁺** and **[2]⁺** is mostly ionic, with a weak covalence degree. We undertook similar analyses on related hypothetical complexes bearing different counter-anions, pincer backbone, and co-ligand in order to investigate how these variables can modulate the Ni-OTf interactions. These studies began by comparing the experimental structure of complex **[1]⁺** to the different structures obtained for the hypothetical complexes in question using various levels of calculation (Figure S4); this exercise allowed us to evaluate the performance of various functionals. We found that the best descriptions of Ni-OTf, Ni-NCCH₃ and N₂C-OTf distances are obtained at the PCM-M06L/Def2TZVP calculation level. The Ni-OTf distance obtained at the PCM-B3PW91/6-31G** calculation level (acetonitrile solvent, $\epsilon = 35.688$) is overestimated by about 0.1 Å relative to the corresponding value found in the solid state structure of complex **[1]⁺**, while the Ni-NCCH₃ and the O5_{triflate}---C1_{imidazolium} distances are underestimated by about 0.05 Å. (See Figure 1 for the atom labelling scheme).

The influence of the calculation level on the topological analysis was also investigated for complex **[1]⁺** (Table 7). The Ni-OTf distances are fairly sensitive to the calculation level, ranging from 2.433 to 2.522, whereas the topological descriptors are fairly insensitive. The PCM-B3PW91/6-31G** level of lower computational cost was, therefore, selected for the theoretical

studies described hereafter.

Table 7. Topological analysis of the Ni-OTf interaction in **[1]⁺** depending on the level of the calculation.

ELF analysis	Ni – OTf (Å)	V(O) ^a	%Ni ^b	Cov. ^c	V(Ni) ^a	ELF	Cov. ^d
Experimental	2.433	2.64	0.02	-0.03	0.29	0.311	-0.17
		3.43	0.01	-0.03			
PCM-M06L/Def2TZVP	2.483	2.72	0.02	-0.01	0.27	0.302	-0.16
		3.37	0.01	-0.01			
PCM-B3PW91/6-31G***	2.522	2.90	0.02	-0.03	0.19	0.300	-0.11
		3.26	0.01	-0.02			

QTAIM analysis	DI	ρ_{bcp}	H_{bcp}	$ H_{\text{bcp}} /\rho_{\text{bcp}}$	$ V_{\text{bcp}} /G_{\text{bcp}}$	E_{int} (kcal/mol)
Experimental	2.433	0.17	-0.028	-0.00117	0.04	10.0
PCM-M06L/Def2TZVP	2.483	0.15	-0.026	-0.001	0.04	8.8
PCM-B3PW91/6-31G***	2.522	0.14	-0.024	0.00018	0.008	7.7

^a: average population \bar{N} of the ELF valence basin (in e^-) ^b: QTAIM atomic contribution of Ni (in e^-) ^c: covariance $\langle \bar{\sigma}^2(V(O), C(\text{Ni})) \rangle$. ^d: covariance $\langle \bar{\sigma}^2(V(\text{Ni}), C(\text{Ni})) \rangle$. B3PW91/6-31G** level of calculation. See main text (section II.2) for the definition of QTAIM BCP descriptors (in a.u.).

III-1. Influence of the counter-anion ($X = \text{TfO}^-$, $(\text{H}_2\text{MeSiO})^-$, $(\text{Me}_2\text{PO}_2)^-$). We have investigated the impact of alternative counter-anions silanolate, $[\text{H}_2\text{MeSiO}]^-$, and phosphinate, $[\text{Me}_2(\text{O})\text{PO}]^-$, on the geometries of the respective complexes **[5]⁺** and **[6]⁺** (Chart 1) and the Ni-O_{anion} interactions found therein. The results of these investigations are presented in Figure 6 and Table 8, and discussed below.

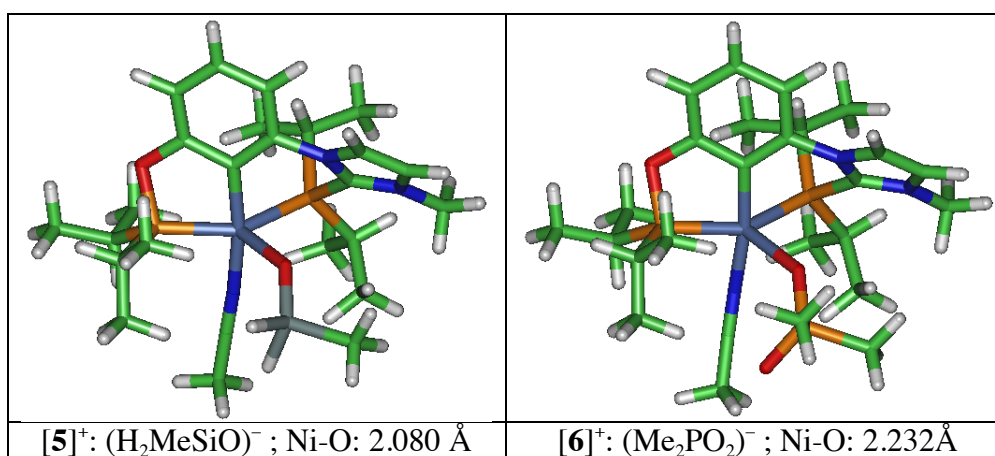


Figure 6. Structures of complexes **[5]⁺** and **[6]⁺** calculated at the PCM-B3PW91/6-31G** level.

Table 8. Selected geometrical data of calculated structures of complexes $[1]^+$ ($X = \text{TfO}^-$), $[5]^+$ ($X = (\text{H}_2\text{MeSiO})^-$) and $[6]^+$ ($X = (\text{Me}_2\text{PO}_2)^-$).

Complex	Anion	ΔE^a	Ni-X (Å)	τ (°)
$[1]^+$	$(\text{CF}_3\text{SO}_3)^-$	6.3	2.522	0.30
$[6]^+$	$(\text{Me}_2\text{PO}_2)^-$	12.7	2.232	0.40
$[5]^+$	$(\text{H}_2\text{MeSiO})^-$	18.5	2.080	0.41

^a Interaction energy (kcal/mol) of the cationic pincer complex with the counter-anion, calculated from equation 2 given in the text. PCM B3PW91/6-31G** level of calculation. Distances are given in Å and angles in degrees.

It is worth noting at the outset that the nature of the counter-anion has little or no bearing on the geometry adopted by the Ni center in these complexes, which can be considered square pyramidal in all cases based on the calculated values of τ (0.30 - 0.41; Table 8). Inspection of the Ni-X distances shown in Figure 6 and Table 8 indicates that the triflate, phosphinate, and silanolate anions are located at about the same distance from the imidazolium ring; in contrast, the Ni-O distances are fairly different and span a relatively wide range (2.080 - 2.522 Å), the phosphinate and silanolate anions being closer to the Ni center. On the basis of the Pauling electronegativity values for Si (1.9), P (2.2), and S (2.6), the weight of the zwitterionic form $\text{E}^+\text{-O}^-$ is expected to be the largest for the silanolate anion. Therefore, the silanolate anion would be expected to display the strongest and shortest Ni-O ionic interaction. The Ni-O interaction energy, ΔE , in the complexes studied was calculated at 0 K (without ZPE correction) at the PCM-B3PW91/6-31G** level (acetonitrile solvent), from equation 2. The results showed that ΔE increases by a factor of 2 or 3, respectively, as the Ni-O distance shrinks from 2.522 Å in $[1]^+$ to 2.232 Å and 2.080 Å.



The ELF topological descriptions of the pincer complexes $[1]^+$, $[5]^+$, and $[6]^+$ appear to be very similar. Thus, the low ELF values, populations, and volumes of $V(\text{Ni})$ are constant along the series (Table 9 and Table S5). Moreover, the total population of $V(\text{O})$ basins is constant along the series, involving about 6 e^- . Nevertheless, there are also some differences among these complexes. For instance, the O atom in the silanolate and phosphinate anions shows one monosynaptic $V(\text{O})$ basin, whereas the triflate O atom in $[1]^+$ has two. Another point of differentiation among the three complexes is the covariance of $V(\text{O})$ with the core basin of nickel $\langle \bar{\sigma}^2(V(\text{O}), C(\text{Ni})) \rangle$, which increases from -0.03 for TfO^- to -0.09 for Me_2PO_2^- and -0.13 for H_2MeSiO^- ; this trend suggests an ionic interaction of increasing covalence degree and strength. This conclusion is also supported by

the results of the QTAIM analysis, showing that the delocalization indices (DI), bond degrees ($|H_{bcp}|/\rho_{bcp}$), and interaction energies (E_{int}) increase accordingly (Table 10 and Table S6).

Table 9. Selected data from ELF analyses performed on complexes $[1]^+$, $[5]^+$, and $[6]^+$. B3PW91/6-31G**//PCM-B3PW91/6-31G** level of calculation.

	$[1]^+$ (CF ₃ SO ₃) ⁻	$[5]^+$ (H ₂ MeSiO) ⁻	$[6]^+$ (Me ₂ PO ₂) ⁻
V(O)	2.90 3.26	6.32	6.12
QTAIM (Ni)	0.02 0.01	0.10	0.06
$\langle \bar{\sigma}^2(V(O),C(Ni)) \rangle$	-0.03 -0.02	-0.13	-0.09
V(Ni)	0.19	0.27	0.30

Table 10. QTAIM descriptors (in a.u.) of the Ni-O bond critical points (BCP) related to the interaction of the nickel atom with the oxygen atom of the counter-anion. B3PW91/6-31G**//PCM-B3PW91/6-31G** level of calculation.

	BCP	DI	ρ_{bcp}	$\Delta\rho_{bcp}$	H_{bcp}	$ H_{bcp} /\rho_{bcp}$	E_{int} (kcal/mol)
$[1]^{+a}$	Ni-OTf	0.17	0.0284	+0.118	-0.00117	0.04	10.0
$[6]^+$	Ni-OP	0.27	0.0462	+0.172	-0.00923	0.20	19.3
$[5]^+$	Ni-Osi	0.39	0.0668	+0.250	-0.01838	0.28	31.2

^a Experimental geometry and B3PW91/6-31G** level of calculation.

The shrinking Ni-O distances along the series $[1]^+ > [6]^+ > [5]^+$ results in increasing DFT and QTAIM interaction energies (Tables 8 and 10). QTAIM interaction energies (E_{int}) are double the DFT interaction energies estimated from equation 2. The observed relative strength and increasing covalence degree of the Ni-O interaction ($[5]^+ > [6]^+ > [1]^+$) is not correlated to the ELF population and volume of V(Ni), as anticipated from the report of de Courcy *et al.*¹⁵

III-2. Influence of the pincer backbone. As discussed above, the Ni-OTf interaction in complexes $[1]^+$ and $[2]^+$ is characterized by a weak covalence degree. In an effort to understand how the nature of the Ni-OTf interaction in these complexes might be influenced by the positive charge present in the imidazoliophosphine moiety of the pincer backbone, the Ni-OTf interactions was studied in two related Ni pincer complexes, one being a charge-neutral compound featuring two phosphinite moieties (**7**) and the other being a dicationic compound featuring two charge-bearing imidazoliophosphine moieties ($[8]^{++}$). It should be noted that $[8]^{++}$ is a hypothetical complex which

has not been prepared yet, whereas **7** is a known species;¹⁰ the experimentally determined structural parameters of the latter will serve as points of comparison to the corresponding parameters obtained from computational studies (Figure 7).

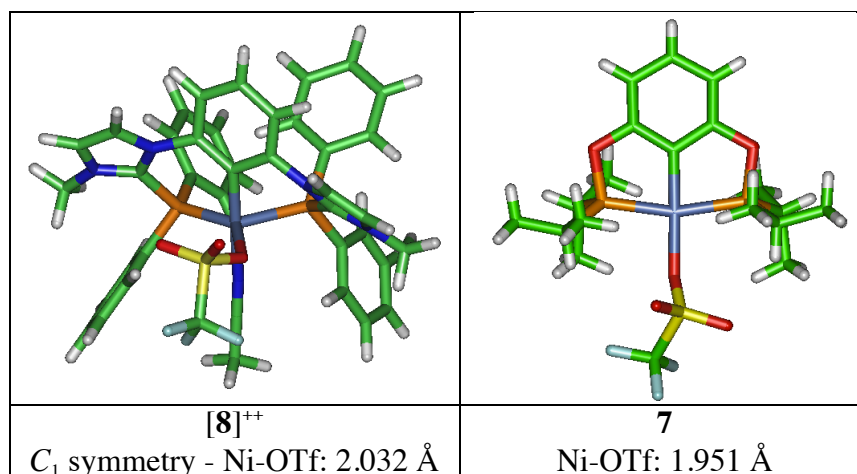


Figure 7. Structures of complexes **7** and **[8]⁺⁺**, calculated at the PCM-B3PW91/6-31G** level.

At the PCM-B3PW91/6-31G** level of calculation, the C_s-symmetric structure of complex **[8]⁺⁺** is a second-order saddle-point, lying 3.7 kcal/mol higher in energy than the structure calculated without symmetry constraints. Unlike complexes **[1]⁺** and **[2]⁺** that adopt a square-pyramidal geometry, complex **[8]⁺⁺** adopts a distorted trigonal bipyramidal arrangement characterized by the large value of the structural parameter $\tau = 0.68$ (Table 11). The calculated Ni-O distances show the following order: 2.032 Å in **[8]⁺⁺**, 2.347 Å in **[2]⁺**, and 2.522 Å in **[1]⁺**. The significantly shorter distance in **[8]⁺⁺** is likely related to the presence of two cationic imidazoliophosphine moieties inducing a stronger electron deficiency of the nickel center. The DFT calculated Ni-OTf interaction energy (ΔE from equation 2) increases along the series **[1]⁺** < **[2]⁺** << **[8]⁺⁺** << and **7** (Table 11).

Table 11. Selected geometrical data for calculated structures of complexes **[1]⁺**, **[2]⁺**, **7**, and **[8]⁺⁺**.^a

	Charge	Pincer	ΔE^b	Ni-OTf (Å)	τ (°)
[1]⁺	+1	^{iPr} PIMIOCOP ^{iPr}	6.3	2.522	0.30
[2]⁺	+1	^{Ph} PIMIOCOP ^{Ph}	8.2	2.347	0.42
[8]⁺⁺	+2	^{Ph} PIMIOCIMIOP ^{Ph}	15.5	2.032	0.68
7	0	^{iPr} POCOP ^{iPr}	29.6	1.938	-

^a PCM-B3PW91/6-31G** level of calculation. Distances are given in Å and angles in degrees. ^b Interaction energy (kcal/mol) of the cationic pincer complex with the triflate counter-anion, calculated from equation 2.

Some notable features of the ELF analysis for **[8]⁺⁺** and **7** include the following:

(i) The population of the monosynaptic V(Ni) basin is larger for **[8]⁺⁺** and **7** (1.83 and 1.64, respectively) relative to the values (about 0.30) found in complexes **[1-6]⁺** (Figure 8, Tables 12 and S7). In the case of **7**, a disynaptic basin V(Ni, P) is evidenced instead of the expected V(Ni) basin, but the small atomic contribution of P to the population of the basin (QTAIM(P) = 0.35) and the large covariance with C(Ni) ($\langle \bar{\sigma}^2(V(\text{Ni}, \text{P}), \text{C}(\text{Ni})) \rangle = -0.93$) suggest that the V(Ni,P) in **7** might be assigned more accurately to the V(Ni) basin (Table 12).

(ii) The number of monosynaptic V(O) basins related to the lone pairs of the triflate oxygen atom vary from one in **[5]⁺** and **[6]⁺** to two in **[1]⁺** and **[2]⁺⁺** and up to three in **7**; according to the report of de Courcy *et al.*,¹⁵ this suggests an increasing covalence degree of the Ni-O bond. This splitting of V(O) into two or three ELF basins is accompanied by a larger QTAIM atomic contribution of Ni to the V(O) basins (0.08 vs 0.03) and by a larger covariance in absolute value ($\langle \bar{\sigma}^2(V(\text{O}), \text{C}(\text{Ni})) \rangle = -0.10$), suggesting a larger covalence degree of the ionic Ni-O bonds in **[8]⁺⁺** and **7** as compared to **[1-6]⁺**.

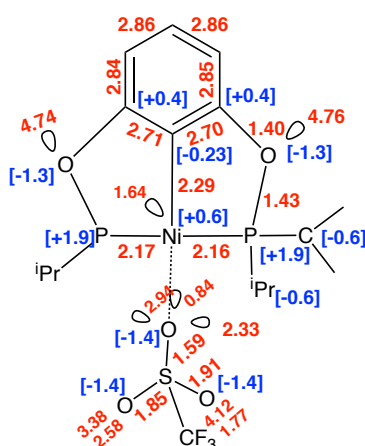


Figure 8. Average populations of selected ELF valence basins (*in red*) and QTAIM atomic charges (*in blue square brackets*) calculated at the B3PW91/6-31G** level for the experimental structure of complex **7**.

Table 13 and Table S7 list the results of a QTAIM analysis on complexes **[1]⁺**, **[8]⁺⁺**, and **7**. Inspection of these results indicates that the covalence degree of the Ni-OTf interaction is much greater in **[8]⁺⁺** relative to **7** and **[1]⁺**: $|\mathbf{H}_{\text{bcp}}|/\rho_{\text{bcp}} = 0.254$ vs. 0.154 vs. 0.04. Indeed, the covalence degree of the Ni-OTf bond is comparable to that of the Ni-NCMe bond in complex **[1]⁺** (Table 4): $|\mathbf{H}_{\text{bcp}}|/\rho_{\text{bcp}} = 0.254$ vs. 0.240; DI = 0.39 vs. 0.57. The covalence degree of the Ni-OTf interaction is thus maximized in complex **[8]⁺⁺** wherein the pincer contains two cationic imidazoliophosphine moieties. On the basis of their E_{int} values, the strength of the Ni-OTf interaction in complexes **[1]⁺**, **[8]⁺⁺**, and **7** follows the order **7** (43.6 kcal/mol) > **[8]⁺⁺** (35.1 kcal/mol) >> **[1]⁺** (10.0 kcal/mol). In

view of de Courcy's assignment of V(O) splitting,²⁵ the greater bond strength and smaller covalence degree of the Ni-OTf in **7** suggest a stronger but more polarized ionic bond in this complex.

Table 12. Selected data of ELF analysis performed at the B3PW91/6-31G**//PCM-B3PW91/6-31G**.

	[1] ⁺ ^a	[8] ⁺⁺ C ₁	7
V(O)	2.64	6.08	0.84
	3.43		2.94
			2.33
QTAIM (Ni)	0.02	0.08	0.04
	0.01		0.02
			0.02
< $\bar{\sigma}^2(\text{V}(\text{O}),\text{C}(\text{Ni}))$ >	-0.03	-0.10	-0.04
	-0.03		-0.03
			-0.03
V(Ni)	0.29	1.83 ^b	1.64

^a Experimental geometry and B3PW91/6-31G** level of calculation. ^b V(Ni, P1), with QTAIM(P1) = 0.35 and < $\bar{\sigma}^2(\text{V}(\text{Ni}, \text{P1}),\text{C}(\text{Ni}))$ > = -0.93.

Table 13. QTAIM characteristics (in a.u.) of the Ni-O bond critical points (BCP) related to the interaction of the nickel atom with the oxygen atom of the triflate counter-anion. B3PW91/6-31G**//PCM-B3PW91/6-31G** level of calculation.

Pincer	DI	ρ_{bcp}	$\Delta\rho_{\text{bcp}}$	H_{bcp}	$ H_{\text{bcp}} /\rho_{\text{bcp}}$	E_{int} (kcal/mol)
[1] ⁺ ^a	0.17	0.0284	+0.118	-0.0012	0.040	10.0
[8] ⁺⁺	0.39	0.071	+0.304	-0.0180	0.254	35.1
7	0.45	0.078	0.464	-0.0120	0.154	43.6

^a: Experimental geometry and B3PW91/6-31G** level of calculation.

III-3. Influence of the in-plane co-ligand. Replacing the acetonitrile ligand in complexes [1]⁺ and [2]⁺ by π -acceptor ligands such as CO, CN-R, and NO⁺ would be expected to render the Ni center in the resulting complexes more electrophilic, and this would, in turn, be anticipated to increase the strength and covalence degree of the Ni-OTf interaction. The nature of the *P*-substituents (R = Ph, *i*-Pr) is also assumed to play a significant role on the nature of the Ni-OTf interaction. To probe these assertions, we carried out computational analyses on the cationic pincer adducts of CO (R = *i*-Pr, [9]⁺, and Ph, [10]⁺), CNCH₃ (R = *i*-Pr, [11]⁺), and NO⁺ (R = *i*-Pr, [12]⁺⁺, and Ph, [13]⁺⁺). (See Chart 1 for line drawings of these adducts.) The results of these analyses confirmed that the introduction of the π -acceptor co-ligands results in the shortening of Ni-O bond distances (Figure 9) and leads to stronger Ni-O interaction energies ΔE , consistent with the increasing electrophilicity of the Ni(II) center (Table 14). One consequence of the shorter Ni-OTf distances is that these

complexes can be considered to be truly pentacoordinated. While the Ni(II) centers in all five complexes adopt variously distorted square pyramidal geometries, it is interesting to note that the τ values range from 0.07 to 0.37 and appear to be sensitive to the nature of the co-ligands (Table 14).

Table 14. Selected geometrical data of calculated structures of complexes $[1]^+$, $[9-11]^+$, $[12-13]^{++}$. PCM-B3PW91/6-31G** level of calculation. Distances are given in Å and angles in degrees.

	L	R	ΔE^a	Ni-OTf	τ
$[1]^+$	MeCN	<i>i</i> -Pr	6.3	2.522	0.30
$[11]^+$	MeNC	<i>i</i> -Pr	6.5	2.398	0.29
$[9]^+$	CO	<i>i</i> -Pr	9.0	2.252	0.31
$[10]^+$	CO	Ph	11.7	2.221	0.37
$[12]^{++}$	NO ⁺	<i>i</i> -Pr	20.1	2.053	0.25
$[13]^{++}$	NO ⁺	Ph	22.1	2.030	0.07

^a Interaction energy (kcal/mol) of the cationic pincer complex with the triflate counter-anion, calculated from equation 2.

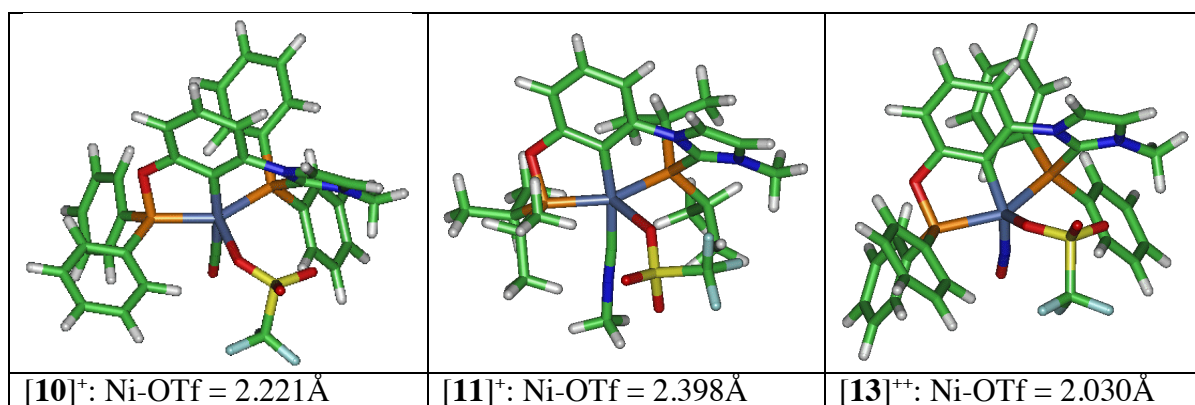


Figure 9. Selected structural data of complexes $[10]^+$ (left), $[11]^+$ (middle) and $[13]^{++}$ (right) calculated at the PCM-B3PW91/6-31G** level in acetonitrile ($\epsilon = 35.688$).

The topological analysis indicates that the covalence degree ($|H_{bcp}|/\rho_{bcp}$), the QTAIM Ni-OTf interaction energy, and the ELF covariance $\langle \sigma^2(V(O),C(Ni)) \rangle$ increase with the electrophilicity of the Ni center (Tables 15 and 16, Tables S9 and S10). In contrast to the previously discussed complexes $[1]^+$, **7** and $[8]^{++}$, the population of V(Ni) in $[9-11]^+$, $[12]^{++}$, and $[13]^{++}$ is not correlated to these covariance values. The covariance $\langle \sigma^2(V(O),C(Ni)) \rangle$ appears thus to be more reliable than the V(Ni) population to estimate the covalence degree of the Ni-OTf ionic interaction.

Table 15. Selected data of ELF analysis performed at the B3PW91/6-31G**//PCM-B3PW91/6-31G** level of calculation.

	[1] ⁺ ^a	[9] ⁺	[10] ⁺	[12] ⁺⁺
V(O)	2.64 3.43	3.71 2.48	6.17	6.20
QTAIM (Ni)	0.02 0.01	0.02 0.03	0.05	0.10
$\langle \bar{\sigma}^2(\text{V(O),C(Ni)}) \rangle$	-0.03 -0.03	-0.04 -0.04	-0.09	-0.13
V(Ni)	0.29	0.30	0.32	1.12

^a Experimental geometry and B3PW91/6-31G** level of calculation.

Table 16. QTAIM characteristics^a (in a.u.) of the Ni-O bond critical points (BCP) related to the interaction of the nickel atom with the oxygen atom of the triflate counter-anion. B3PW91/6-31G**//PCM-B3PW91/6-31G** level of calculation.

	L	DI	ρ_{bcp}	$\Delta\rho_{\text{bcp}}$	H_{bcp}	$ H_{\text{bcp}} /\rho_{\text{bcp}}$	E_{int} (kcal/mol)
[1] ⁺ ^a	MeCN	0.17	0.0284	+0.118	-0.0012	0.04	10.0
[9] ⁺	CO	0.26	0.044	0.167	-0.0080	0.181	18.2
[10] ⁺	CO	0.26	0.046	0.180	-0.0090	0.196	19.5
[12] ⁺⁺	NO ⁺	0.39	0.070	0.270	-0.0190	0.271	33.3

^a Experimental geometry and B3PW91/6-31G** level of calculation.

IV. Comparative ELF, QTAIM and EDA analyses of the covalence degree of the Ni-X interaction

IV-1. QTAIM analysis. The most relevant QTAIM descriptors of the Ni-OTf interaction for all complexes are shown in Table 17, arranged according to decreasing Ni-O distances. The large positive value for the Laplacian of the electron density at the BCP ($\Delta\rho_{\text{bcp}}$) and the small negative values of the energy density at the BCP (H_{bcp}) are in favor of an ionic Ni-OTf bond with a tunable covalence degree. The shorter the Ni-O distance, the larger the electron density and the Laplacian, the larger the delocalization index (DI) related to the covalence degree and multiplicity of the bond, the covalence degree ($|H_{\text{bcp}}|/\rho_{\text{bcp}}$) and the QTAIM interaction energy (E_{int}) (Table 17). It is worth noting here that the complex **7** featuring the charge-neutral POCOP ligand is the only complex in the series for which E_{int} and $\Delta\rho_{\text{bcp}}$ are not correlated with the covalence degree $H_{\text{bcp}}/\rho_{\text{bcp}}$.

Table 17. QTAIM descriptors in au, calculated at the B3PW91/6-31G**//PCM-B3PW91/6-31G** level.

	Ni-O (Å)	DI	ρ_{bcp}	$\Delta\rho_{\text{bcp}}$	H_{bcp}	$ H_{\text{bcp}}/\rho_{\text{bcp}} $	$E_{\text{int}}^{\text{int}}$ (kcal/mol)
[1] ⁺ ^a	2.433	0.17	0.028	0.118	-0.001	0.036	10.0
[1] ⁺ ^b	2.484	0.15	0.026	0.107	-0.001	0.038	8.8
[9] ⁺	2.253	0.26	0.044	0.167	-0.008	0.181	18.2
[6] ⁺	2.232	0.27	0.046	0.172	-0.009	0.200	19.3
[10] ⁺	2.221	0.26	0.046	0.180	-0.009	0.196	19.5
[5] ⁺	2.080	0.39	0.067	0.250	-0.018	0.271	33.3
[12] ⁺⁺	2.053	0.39	0.070	0.270	-0.019	0.271	33.3
[8] ⁺⁺	2.032	0.39	0.071	0.304	-0.018	0.280	31.2
7	1.951	0.45	0.078	0.464	-0.012	0.154	43.6

^a Experimental geometry and B3PW91/6-31G** level of calculation. ^b B3PW91/6-31G**//PCM-M06L/Def2TZVP level of calculation.

The modulation of the covalence degree of the Ni-O ionic interaction can thus be achieved in several ways. Strongest covalence degrees are obtained by exchanging the triflate by a silanolate anion, the CH₃CN by an in plane NO⁺ co-ligand, or by introducing in the pincer ligand a second positively charged imidazoliophosphine donor moiety.

IV-2. Energy decomposition analysis (EDA). In agreement with the ionic character of the Ni-OTf bond indicated by the QTAIM analyses discussed above, a significant ionic contribution is emphasized from EDA analysis as illustrated in Table 18 by both ratios $E_{\text{int}} / E_{\text{elstat}}$ and $E_{\text{int}} / E_{\text{attr}}$, larger than 80 and 90%, respectively. For complex [1]⁺, the low value of the sum $E_{\text{Pauli}} + E_{\text{orb}}$ related to the overall orbital contribution (destabilizing + stabilizing) is also in favor of an ionic Ni-O bond. The stronger covalence degree of the Ni-O bond reaches its maximum in complexes [10]⁺ and [13]⁺⁺, as indicated by the calculated larger $E_{\text{Pauli}} + E_{\text{orb}}$ values. The intermediate value of the sum $E_{\text{Pauli}} + E_{\text{orb}}$ obtained for complex **7** suggests the presence of a stronger ionic bond than in complexes [10]⁺ and [13]⁺⁺, but with a lower covalence degree, in agreement also with the QTAIM studies.

Table 18. EDA analyses of complexes [1]⁺, **7**, [10]⁺ and [12]⁺⁺. Energies (kcal/mol) calculated at the PBE/TZP level for geometries optimized at the PCM-B3PW91/6-31G** level of calculation.

	Ni – O	E_{int}	E_{Pauli}	E_{elstat}	E_{orb}	$E_{\text{int}}/E_{\text{attr}}$	$E_{\text{int}}/E_{\text{elstat}}$	$E_{\text{Pauli}} + E_{\text{orb}}$
[1] ⁺	2.522	-131.44	25.12	-134.34	-22.22	0.86	0.98	2.90
[1] ⁺ ^a	2.433	-130.5	26.97	-135.28	-22.19	0.86	0.96	4.78
[10] ⁺	2.253	-141.35	46.16	-152.91	-34.6	0.90	0.92	11.56
[12] ⁺⁺	2.053	-225.35	77.31	-244.45	-58.21	0.82	0.92	19.10
7 ^a	1.951	-112.75	60.40	-128.66	-44.49	0.81	0.87	15.91

^a Experimental geometry.

MO analysis of $[1]^+$ has revealed an MO (#163 in Figure 10) showing a σ -bonding overlap between the atomic orbitals of Ni (hybrid sd) and a p atomic orbital of the triflate oxygen atom. Another MO (#161 in Figure 10) appears to be related to the π - or δ -interaction between these two fragments as it shows the bonding overlap $d(\text{Ni}) - p(\text{O})$.

For complex **7**, no σ -bonding overlap between the atomic orbitals of Ni and of the triflate oxygen atom could be found. MOs #124 and #137 (Figure 10) appear to be related to the π - or δ -interaction between these two fragments as they exhibit a lateral bonding overlap $d(\text{Ni}) - p(\text{O})$.

However, for both complexes, the corresponding anti-bonding overlaps could not be found in the MO diagram. These MOs interactions may be therefore rather related to repulsive interactions between occupied MOs in agreement with the large positive values of $(E_{\text{Pauli}} + E_{\text{orb}})$ energies calculated within EDA analysis (Table 18).

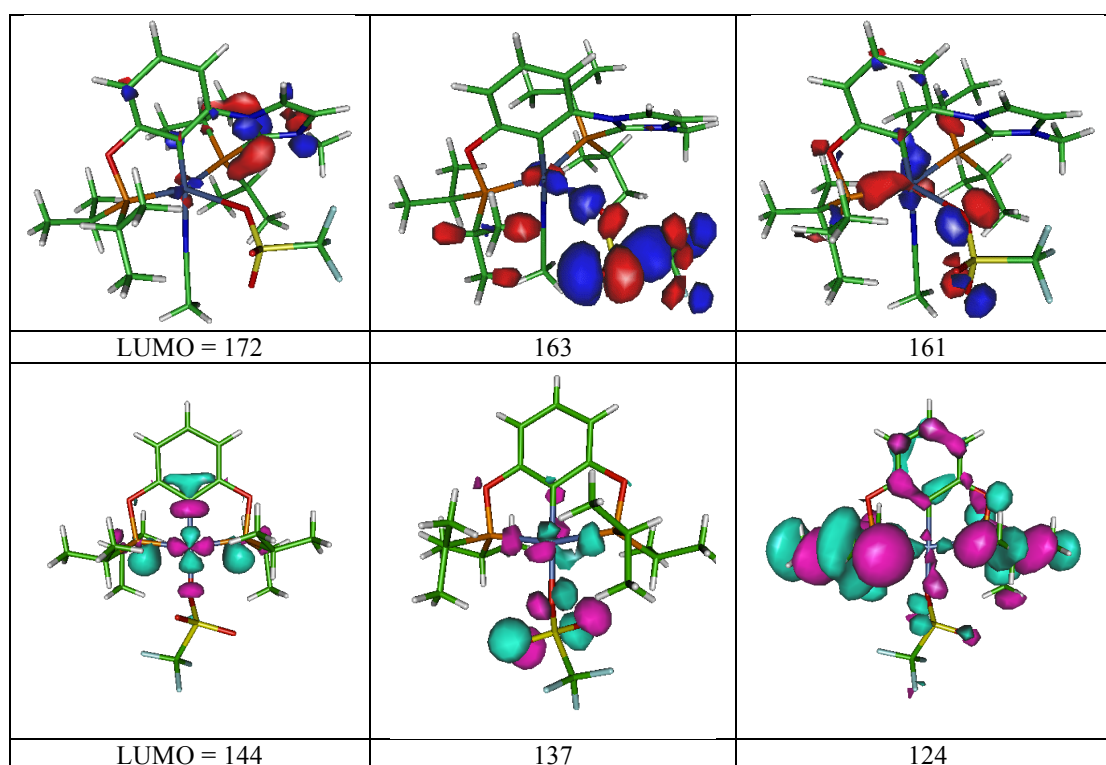


Figure 10. Molecular orbitals of $[1]^+$ (*top*) and **7** (*bottom*). B3PW91/6-31G** level of calculation.

IV-3. ELF analysis. The most relevant ELF descriptors of the Ni-OTf interaction for all complexes are shown in Table 19; the complexes studied are listed according to decreasing Ni-O distances. All descriptors are consistent with the presence of an ionic bond with a sizeable covalence degree, in agreement with QTAIM and EDA analyses. The subvalence monosynaptic $V(\text{Ni})$ basin is the ELF signature of the weak covalence degree of the Ni-OTf ionic bond. However, little variation of both the population and of the volume of $V(\text{Ni})$ are observed with the covalence degree of the ionic Ni-OTf bond. As already mentioned above, the QTAIM atomic contribution of Ni and the absolute

value of the covariance $\langle \bar{\sigma}^2(V(O),C(Ni)) \rangle$ appear to be more reliable for quantifying the covalence degree of the ionic interaction.

Table 19. ELF selected data calculated at the B3PW91/6-31G**//PCM-B3PW91/6-31G**.

	Ni-O (Å)	V(Ni)	V(O)	QTAIM(Ni)	$\langle \bar{\sigma}^2(V(O),C(Ni)) \rangle$	V(O) #
[1] ⁺ ^a	2.433	0.29	2.64	0.02	-0.03	2
[1] ⁺ ^b	2.484	0.27	2.72	0.02	-0.03	2
[9] ⁺	2.253	0.30	2.48	0.03	-0.04	2
[6] ⁺	2.232	0.30	6.12	0.06	-0.09	1
[10] ⁺	2.221	0.32	6.17	0.05	-0.09	1
[5] ⁺	2.080	0.27	6.32	0.10	-0.13	1
[12] ⁺⁺	2.053	1.12	6.20	0.10	-0.13	1
[8] ⁺⁺	2.032	1.83	6.08	0.08	-0.10	1
7	1.951	1.64	0.84	0.04	-0.04	3

^a B3PW91/6-31G** (experimental geometry) level of calculation. ^b B3PW91/6-31G**//PCM-M06L/Def2TZVP level of calculation.

Conclusions

This study has strived to provide a detailed characterization of the pentacoordinated Ni(II) centers in a series of cationic PCP pincer complexes, the pentacoordination resulting from an apical Ni-O interaction with the oxygen atom of one of the counter anions. Theoretical studies have shown that the covalence degree of the Ni-O ionic interaction may be modulated through several ways, the strongest covalence degrees resulting from the exchange of the triflate by a silanolate anion and the acetonitrile by an axial nitrosyl co-ligand, or by introducing a second cationic peripheral extremity to the pincer ligand. The pentacoordination of the nickel center results in a distorted square pyramidal geometry. However, the geometry index τ measuring the extent of the distortion is almost constant, lying in the 0.2-0.4 range over the series of complexes **1-13**; in other words, this parameter is not related to the strength of the Ni-O interaction.

In agreement with previous reports of de Courcy *et al.*,¹⁵ the subvalence V(Ni) basin is shown here to be the ELF signature of the weak covalence degree of the Ni-OTf ionic bond in all complexes studied. However, the population and volume of V(Ni) could not be used to quantify the covalence degree of the Ni-O ionic interaction. The latter is better quantified by the absolute value of ELF covariances $\langle \bar{\sigma}^2(V(O),C(Ni)) \rangle$ or QTAIM delocalization indices (DI). Linear correlations of the Ni-O distance or the QTAIM interaction energy with QTAIM DIs, bond degrees and ELF covariances are evidenced (Figure 11). Linear correlations with the same slope between various QTAIM descriptors of the covalence degree are noticeable.

The Ni-O interaction observed between the triflate anion, the cationic Ni center, and the imidazolium ring suggest a possible control of the selectivity of catalytic processes involving charged substrates. This possibility will be investigated in future studies.

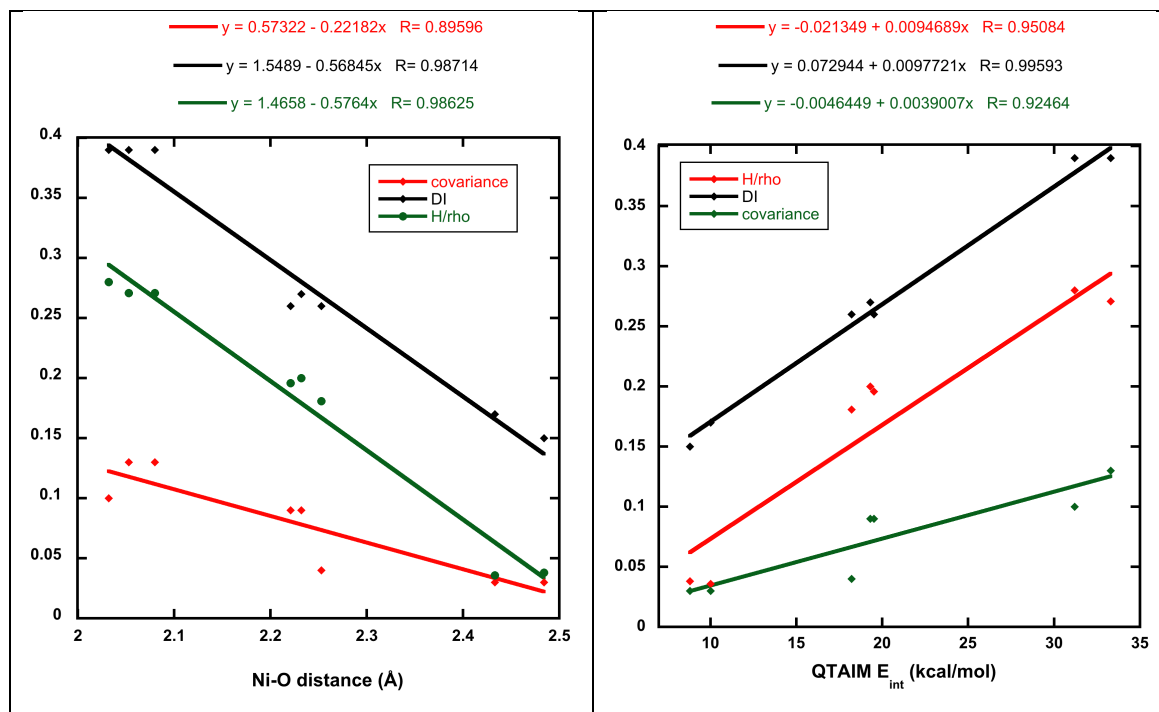


Figure 11. Linear correlations between ELF and QTAIM descriptors of the covalence degree of the ionic Ni-OTf interaction.

Computational details

Geometries were fully optimized at the PCM-B3PW91/6-31G** or PCM-B3PW91/6-31G** LANL2DZ*(Ni) level of calculation using Gaussian09.²⁶ LANL2DZ*(Ni) means that f-polarization functions derived by Ehlers *et al.*²⁷ for Ni, have been added to the LANL2DZ(Ni) basis set. Vibrational analysis was performed at the same level as the geometry optimization. Solvent effects were included using the polarizable continuum model (PCM) implemented in Gaussian09 for acetonitrile ($\epsilon = 35.688$).

Electron Localization Function (ELF)²⁸ topological analysis and Quantum Theory of Atoms in Molecules (QTAIM)²⁹ analysis were performed with the TopMoD package.¹² ELF maps were plotted using the Molekel program.³⁰ QTAIM analysis was also performed with the AIMAll software.³¹

Topological analyses. Topological methods are based on the analysis of the gradient field of a local function within the dynamic field theory and provide a partition of the molecular space into non-overlapping basins.

The topological analysis of the electron density $\rho(r)$, designed as the Quantum Theory of Atoms in Molecules (QTAIM) by R. Bader, yields atomic basins and QTAIM atomic charges.²⁹ It allows defining bond paths and bond critical points (BCP). The nature of the chemical bond is characterized from various properties of the electron density at the BCPs, especially the sign of the Laplacian of the electron density and the values of energy densities $H_{bcp} = G_{bcp} + V_{bcp}$ following the Macchi's classification.¹⁹ The covalence degree may be estimated from H_{bcp}/ρ_{bcp} .²¹ The strength of the interaction may be estimated from the correlation scheme of Espinosa *et al.* and the corresponding interaction energy (E_{int}).²² The reliability of these QTAIM interaction energies (E_{int}) has been discussed in the literature.³² QTAIM interaction energies (E_{int}) were indeed disclosed for describing weak hydrogen bonds. They have been successfully used for investigating other weak, strong or medium strength non-covalent interactions.^{32,33} However, their values might be less reliable for comparing stronger dative bonds. It is noticeable however that a very good agreement between E_{int} values of Au-PPh₃ bonds and the corresponding calculated dissociation energies³⁴ on the one hand and between E_{int} values of Gd-OH₂ bonds and sublimation enthalpies measurements³⁵ on the other hand were reported.

The electron localization function (ELF) measures the excess of kinetic energy due to the Pauli repulsion.²⁸ ELF values are confined between 0 and 1. ELF is close to 1 in regions where electrons are single or form antiparallel spin pairs, whereas it tends to 0 in regions where the probability to find parallel spin electrons close to one another is high.²⁸ ELF tends to a value of 1 in those regions where the electron localization is high (atomic shells, chemical bonds, and lone electron pairs),³⁶ whereas it tends toward small values at the boundaries between these regions.³⁷ The topological analysis of the ELF gradient field yields a partition of the molecular space into non-overlapping electronic domains, classified into core, valence bonding and nonbonding basins. These basins are in one-to-one correspondence to the core, lone or shared pairs of the Lewis model. A core basin contains a nucleus X (except a proton) and is designated as C(X). A valence bonding basin lies between two or more core basins. Valence basins are further distinguished by their synaptic order, which is the number of core basins with which they share a common boundary. The monosynaptic basins denoted as V(X), correspond to lone pairs, whereas the di- and polysynaptic ones are related to bi- or multi-centric bonds, denoted as V(X1, X2, X3, ...). The average population of the basin is obtained by integration of the one-electron density over the basin volume. These populations do not take integral values and are about twice the topologically defined Lewis bond orders for bonding valence basins. The populations and (co)variances of these valence basins can be further interpreted in terms of weighted combinations of mesomeric structures.³⁸

Energy decomposition analyses were performed using the optimized or experimental structures and the ADF2013 package,³⁹ following the implemented Morokuma-Rauk-Ziegler

partition scheme²³ and using the PBE functional in combination with Slater-type (STO) all-electron basis sets of TZP quality including scalar relativistic effects.⁴⁰ Vibrational analysis was performed at the same level as the geometry optimization. Solvent effects were included using the conductor-like screening model (COSMO)⁴¹ implemented in ADF 2013.³⁹

Molecular orbitals were plotted using the GABEDIT program.⁴²

Supplementary Information.

Crystallographic information for complexes **1-3** and complementary computational data.

Acknowledgements. The theoretical studies were performed using HPC resources from CALMIP (Grant 2013-2018 [0851]) and from GENCI-[CINES/IDRIS] (Grant 2013-2018 [085008]). The authors gratefully acknowledge the financial support provided by NSERC (Discovery grant to DZ) and FRQNT (Ph. D. fellowship to BV). The Direction des Relations Internationales of Université de Montréal and Université Toulouse 3-Paul Sabatier are gratefully acknowledged for the travel grants that made this collaborative project possible. The authors would like to thank Professor Bernard Silvi for fruitful discussions.

Notes and References

- ¹ (a) Crabtree RH (2005) 4th ed.; Hoboken, New Jersey: Wiley pp 35. (b) Huheey JE, Keiter EA, Keiter, LR (1993) 4th ed.; New York: Harper Collins College pp 936.
- ² Roddick DM, Zargarian D (2014) *Inorg Chim Acta* 422:251-264.
- ³ (a) Hope H, Olmstead MM, Power PP, Viggiano M (1984) *Inorg Chem* 23:326-330. (b) Stalick JK, Ibers JA (1969) *Inorg Chem* 8:1084-1090. (c) Klein HF, Dal A, Jung T, Flörke U, Haupt HJ (1998) *Eur J Inorg Chem* 2027-2032. (d) Klein HF, Zwiener M, Petermann A, Jung T, Cordier G, Hammerschmitt B, Flörke U, Haupt HJ, Dartiguenave Y (1994) *Chem Ber* 127:1569-1578.
- ⁴ (a) Vabre B, Canac Y, Duhayon C, Chauvin R, Zargarian D (2012) *Chem Commun* 48: 10446-10448. (b) Vabre B, Canac Y, Lepetit C, Duhayon C, Chauvin R, Zargarian D (2015) *Chem Eur J* 21:17403-17414.
- ⁵ Wu S, Li X, Xiong Z, Xu W, Lu Y, Sun H (2013) *Organometallics* 32:3227-3237.
- ⁶ A series of pentacoordinated pincer complexes of the type (PCP)Ni(*o*-semiquinonato) has been shown to adopt square pyramidal geometry, but there is some ambiguity about whether these paramagnetic compounds should be considered trivalent (17-electron) or divalent (18-electron) species. (a) Kozhanov KA, Bubnov MP, Vavilina NN, Efremova LY, Fukin GK, Cherkasov VK, Abakumov GA (2009) *Polyhedron* 28:2555-2558. (b) Kozhanov KA, Bubnov MP, Cherkasov VK, Vavilina NV, Efremova LY, Artyushin OI, Odinets IL, Abakumov GA (2008) *Dalton Trans* 2849-2853. (c) Kozhanov KA, Bubnov MP, Cherkasov VK, Fukin GK, Abakumov GA (2003) *Chem Commun* 2610. (d) Kozhanov KA, Bubnov MP, Cherkasov VK, Fukin GK, Abakumov GA (2004) *Dalton Trans* 2957-2962.
- ⁷ The coordination plane in question is the least-squares plane defined by P1, C5, P2, and N3 in the acetonitrile adducts and by P1, C5, P2, O8 in the aquo adduct.
- ⁸ The τ index is commonly used to categorize the geometry of a 5-coordinated species. Defined by the equation $(\beta - \alpha)/60$ where β and α (in degrees) are the two largest valence angles of the coordination center ($\beta > \alpha$), τ takes numerical values ranging from 0 (for an ideal square pyramidal geometry) to 1 (for an ideal trigonal bipyramidal geometry). The extent of distortion from the two ideal geometries can thus be estimated from the τ value calculated for a given 5-coordinated complex. For a discussion of τ index see: Addison AW, Rao NT, Reedijk J, van Rijn J, Verschoor GC (1984) *J Chem Soc Dalton Trans* 1349-1355.
- ⁹ Zargarian D, Castonguay A, Spasyuk DM (2013) *Top Organomet Chem* 40:131-174. Eds. G. van Koten and D. Milstein, Springer Verlag, Berlin Heidelberg.
- ¹⁰ Salah A, Offenstein C, Zargarian D (2011) *Organometallics* 30:5352-5364.
- ¹¹ The complete set of ELF data for complex [1]⁺⁺ is presented in the Electronic Supporting Information of reference 4b.

-
- ¹² Noury S, Krokidis X, Fuster F, Silvi B (1999) *Computers and Chemistry* 23:597-604.
- ¹³ This approach for estimating the formal oxidation number using ELF analysis was successfully applied to ambiguous cases and the results were nicely correlated to the X-ray Photoelectron Spectroscopy results. See Andres J, Feliz M, Fraxedas J, Hernandez V, Lopez-Navarrete JT, Llusar R, Sauthier G, Sensato FR, Silvi B, Bo C, Campanera JM (2007) *Inorg Chem* 46 :2159-2166.
- ¹⁴ The population of V(Ni) is insensitive to the accuracy level of the ELF analysis (grid size, approximation in the gradient field analysis), the location of the V(Ni) attractor, the volume and the V(Ni) population depend on the type of double zeta basis set (6-31G**, 6-31++G**, DGDZVP, ...). See Table S1 in SI.
- ¹⁵ (a) De Courcy B, Dognon J-P, Clavaguéra C, Gresh N, Piquemal J.-P. (2011) *Int J Quant Chem* 111:1213-1221. (b) B. de Courcy, L. G. Pedersen, O. Parisel, N. Gresh, B. Silvi, J. Pilmé, J.-P. Piquemal., (2010) *J Chem Theor Comput* 6:1048-1063.
- ¹⁶ (a) Bader RFW (1990) in *Atoms In Molecules*; Clarendon Press: Oxford, UK. (b) Bader RFW, Essen H (1984) *J Chem Phys* 80:1943-1960.
- ¹⁷ Bianchi R, Gervasio G, Marabello D (2000) *Inorg Chem* 39:2360-2366.
- ¹⁸ Lepetit C, Fau P, Fajerweg K, Kahn ML, B. Silvi B (2017) *Coord Chem Rev* 345:150-181.
- ¹⁹ Macchi P, Proserpio DM, Sironi A (1998) *J Am Chem Soc* 120:13429-13435.
- ²⁰ For a classification of various ligands see: Green, MLH (1995) A new approach to the formal classification of the covalent compounds of the elements. *J Organomet Chem* 500:127-148.
- ²¹ Espinosa E, Alkorta I, Elguero J, Molins E (2002) *J Chem Phys* 117:5529-5542.
- ²² $E_{\text{int}} = \frac{1}{2} V_{\text{bcp}}$ and $E_{\text{int}} \text{ (kcal/mol)} = -313.754 \times V_{\text{bcp}} \text{ (au)}$. See (a) Espinosa E, Molins E, Lecomte C (1998) *Chem Phys Lett* 285:170-173. (b) Espinosa E, I. Alkorta I, I. Rozas I, J. Elguero J, E. Molins E (2001) *Chem Phys Lett* 336:457-461.
- ²³ (a) Ziegler T, Rauk A (1979) *Inorg Chem* 18:1558-1565. (b) Ziegler T, Rauk A (1979) *Inorg Chem* 18: 1755-1759 (c) Bickelhaupt FM, Baerends E J (2000) in *Rev. Comput. Chem.*; Lipkowitz KB and Boyd, DB Eds.; Wiley, New York 15:1-86.
- ²⁴ Jacobsen H, Correa A, Poater A, Costabile C, Cavallo L (2009) *Coord Chem Rev* 253:687-703.
- ²⁵ According to reference [15], the electrostatic interaction between the metallic cation and the ligand is more polarized or covalent, when the number of monosynaptic basins describing the lone pair of the ligand increase. As a result, because of the differential polarizing field surrounding it, the cation splits its outer-shell density towards the ligands into localization domains called subvalence basins whose volume and population increase as the nature of the interaction becomes more covalent/polarized.

-
- ²⁶ Gaussian 09, Revision D.01, M. J. Frisch, G. W. Trucks, H. B. Schlegel, G. E. Scuseria, M. A. Robb, J. R. Cheeseman, G. Scalmani, V. Barone, B. Mennucci, G. A. Petersson, H. Nakatsuji, M. Caricato, X. Li, H. P. Hratchian, A. F. Izmaylov, J. Bloino, G. Zheng, J. L. Sonnenberg, M. Hada, M. Ehara, K. Toyota, R. Fukuda, J. Hasegawa, M. Ishida, T. Nakajima, Y. Honda, O. Kitao, H. Nakai, T. Vreven, J. A. Montgomery, Jr., J. E. Peralta, F. Ogliaro, M. Bearpark, J. J. Heyd, E. Brothers, K. N. Kudin, V. N. Staroverov, R. Kobayashi, J. Normand, K. Raghavachari, A. Rendell, J. C. Burant, S. S. Iyengar, J. Tomasi, M. Cossi, N. Rega, J. M. Millam, M. Klene, J. E. Knox, J. B. Cross, V. Bakken, C. Adamo, J. Jaramillo, R. Gomperts, R. E. Stratmann, O. Yazyev, A. J. Austin, R. Cammi, C. Pomelli, J. W. Ochterski, R. L. Martin, K. Morokuma, V. G. Zakrzewski, G. A. Voth, P. Salvador, J. J. Dannenberg, S. Dapprich, A. D. Daniels, Ö. Farkas, J. B. Foresman, J. V. Ortiz, J. Cioslowski, and D. J. Fox, Gaussian, Inc., Wallingford CT, 2009.
- ²⁷ Ehlers AW, Böhme M, Dapprich S, Gobbi A, Höllwarth A, Jonas V, Köhler KF, Stegmann R, Veldkamp A, Frenking G (1993) *Chem Phys Lett* 208:111-114.
- ²⁸ (a) Becke AD, Edgecombe KE (1990) *J Chem Phys* 92:5397-5403; (b) Silvi B, Savin A (1994) *Nature*, 371:683-686.
- ²⁹ Bader RFW (1990) in *Atoms In Molecules* Clarendon Press: Oxford, UK.
- ³⁰ Molekel 4.3 from CSCS: <http://www.cscs.ch/molekel/>
- ³¹ Keith TA, AIMAll (Version 16.01.09), TK Gristmill Software, Overland Park KS, USA, 2016 (aim.tkgristmill.com).
- ³² (a) Spackman MA (2015) *Cryst Growth Des* 15:5624–5628. (b) Nelyubina YV, Antipin MY, Lyssenko KA (2010) *Russ Chem Rev* 79:167-187. (c) Gatti C (2005) *Z Kristallogr - Cryst Mater* 220:399–457.
- ³³ Valyaev DA, Brousses R, Lugan N, Fernández I, Sierra MA (2011) *Chem Eur J* 17:6602 – 6605.
- ³⁴ Borissova AO, Korlyukov AA, Antipin MY, Lyssenko KA (2008) *J Phys Chem A* 112 :11519–11522.
- ³⁵ Puntus LN, Lyssenko KA, Antipin MY, Bünzli JCG (2008) *Inorg Chem* 47 :1105-11107.
- ³⁶ Poater J, Duran M, Sola M, Silvi B (2005) *Chem Rev* 105:3911-3947.
- ³⁷ Silvi B, Gillespie RJ, Gatti. C (2013) in *Comprehensive Inorganic Chemistry II* 9:187-226.
- ³⁸ (a) Lepetit C, Silvi B, Chauvin R (2003) *J Phys Chem A* 107:464-473. (b) Silvi B (2004) *Phys Chem Chem Phys* 6:256-260.
- ³⁹ (a) te Velde G, Bickelhaupt FM, van Gisbergen SJA, Fonseca Guerra C, Baerends EJ, Snijders JG, Ziegler T (2001) *J Comp Chem* 22: 931-967 (b) Fonseca Guerra C, Snijders JG, te Velde G, Baerends EJ (1998) *Theor Chem Acc* 99:391-403. (c) ADF2013, SCM, Theoretical Chemistry, Vrije Universiteit, Amsterdam, The Netherlands, <http://www.scm.com>.

Optionally, you may add the following list of authors and contributors:

E.J. Baerends, T. Ziegler, J. Autschbach, D. Bashford, A. Bérces, F.M. Bickelhaupt, C. Bo, P.M. Boerrigter, L. Cavallo, D.P. Chong, L. Deng, R.M. Dickson, D.E. Ellis, M. van Faassen, L. Fan, T.H. Fischer, C. Fonseca Guerra, M. Franchini, A. Ghysels, A. Giammona, S.J.A. van Gisbergen, A.W. Götz, J.A. Groeneveld, O.V. Gritsenko, M. Grüning, S. Gusarov, F.E. Harris, P. van den Hoek, C.R. Jacob, H. Jacobsen, L. Jensen, J.W. Kaminski, G. van Kessel, F. Kootstra, A. Kovalenko, M.V. Krykunov, E. van Lenthe, D.A. McCormack, A. Michalak, M. Mitoraj, S.M. Morton, J. Neugebauer, V.P. Nicu, L. Noodleman, V.P. Osinga, S. Patchkovskii, M. Pavanello, P.H.T. Philipsen, D. Post, C.C. Pye, W. Ravenek, J.I. Rodríguez, P. Ros, P.R.T. Schipper, G. Schreckenbach, J.S. Seldenthuis, M. Seth, J.G. Snijders, M. Solà, M. Swart, D. Swerhone, G. te Velde, P. Vernooijs, L. Versluis, L. Visscher, O. Visser, F. Wang, T.A. Wesolowski, E.M. van Wezenbeek, G. Wiesenekker, S.K. Wolff, T.K. Woo, A.L. Yakovlev.

⁴⁰ Van Lenthe E, Baerends EJ (2003) *J Comp Chem* 24:1142-1156.

⁴¹ Pye CC, Ziegler T (1999) *Theor Chem Acc* 101:396-408.

⁴² <http://sites.google.com/site/allouchear/Home/gabedit>.

SUPPORTING INFORMATION

For

Pentacoordinated, Square-Pyramidal Cationic PCP Ni(II) Pincer Complexes: ELF and QTAIM Topological Analyses of Nickel-Triflate Interactions

Christine Lepetit,^{*a} Boris Vabre,^b Yves Canac,^{*a} Mohammad Esmail Alikhani,^{*c}
and Davit Zargarian^{*b}

[a] LCC-CNRS, Université de Toulouse, CNRS, Toulouse, France.

[b] Département de Chimie, Université de Montréal, Montréal, Québec H3C 3J7, Canada.

[c] Sorbonne Universités, UPMC Université Paris 06, MONARIS, UMR 8233, Université Pierre et Marie Curie, 4 Place Jussieu, Case courrier 49, F-75252 Paris Cedex 05, France.

E-mail: christine.lepetit@lcc-toulouse.fr, yves.canac@lcc-toulouse.fr, esmail.alikhani@sorbonne-universite.fr, zargarian.davit@umontreal.ca

Table of contents

Page 2: Figures S1 and S2

Page 3: Figure S3 and S4

Page 4: Table S1

Page 5: Tables S2-S4

Page 6: Tables S5 and S6

Page 7: Tables S7 and S8

Page 8: Tables S9 and S10

Page 9: Crystallographic information for complexes **1**, **2** and **3**

Page 10: Table S11

Page 11: References

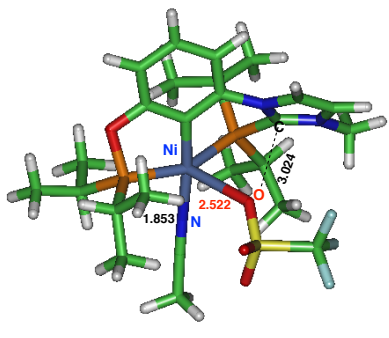
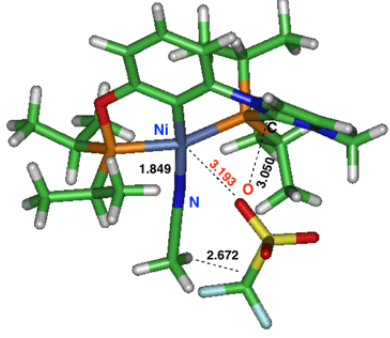
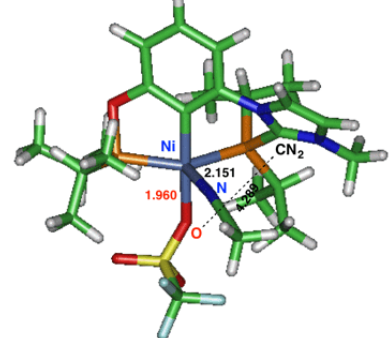
		
Calc. (0.0) Ni-O Tf : 2.522 Å N ₂ C-O Tf : 3.024 Å Ni-N(CCH ₃): 1.853 Å	Calc. (+ 2.7) Ni-O Tf : 3.193 Å N ₂ C-O Tf : 3.05 Å Ni-N(CCH ₃): 1.849 Å	Calc. (+ 8.4) Ni-O Tf : 1.960 Å N ₂ C-O Tf : 4.289 Å Ni-N(CCH ₃): 2.151 Å

Figure S1. Selected calculated geometrical data for various isomers of ⁱPrPIMIOCOPⁱPr pincer Ni complex **1**. (*Left*) experimental conformation of **1**, (*middle*) orientation of the triflate anion identical to the one in the experimental structure of **2**, (*right*) isomer of **1** built by inversion of acetonitrile ligand and triflate anion positions. Relative energies (in kcal/mol) in bold and brackets. PCM-B3PW91/6-31G** level of calculation (acetonitrile solvent, $\epsilon = 35.688$).

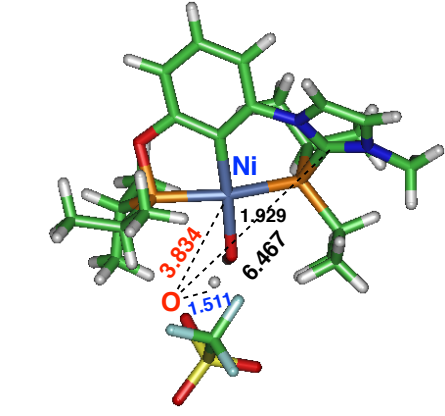
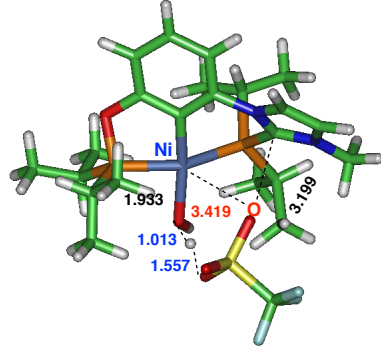
	
Calcd. (0.0) Ni-O Tf : 3.834 Å et N ₂ C-O Tf : 6.467 Å Ni-O(H) ₂ : 1.929 Å Hydrogen bond: 1.511 Å	Calcd. (+ 1.2) Ni-O Tf : 3.419 Å et N ₂ C-O Tf : 3.199 Å Ni-O(H) ₂ : 1.933 Å Hydrogen bond: 1.557 Å

Figure S2. Selected calculated geometrical data for the ⁱPrPIMIOCOPⁱPr pincer Ni complex **3**: (*left*) orientation of the triflate anion identical to the one of the experimental structure, (*right*) orientation of the triflate anion identical to the one of complex **1**. Relative energies (in kcal/mol) in bold and brackets. PCM-B3PW91/6-31G** level of calculation (acetonitrile solvent, $\epsilon = 35.688$).

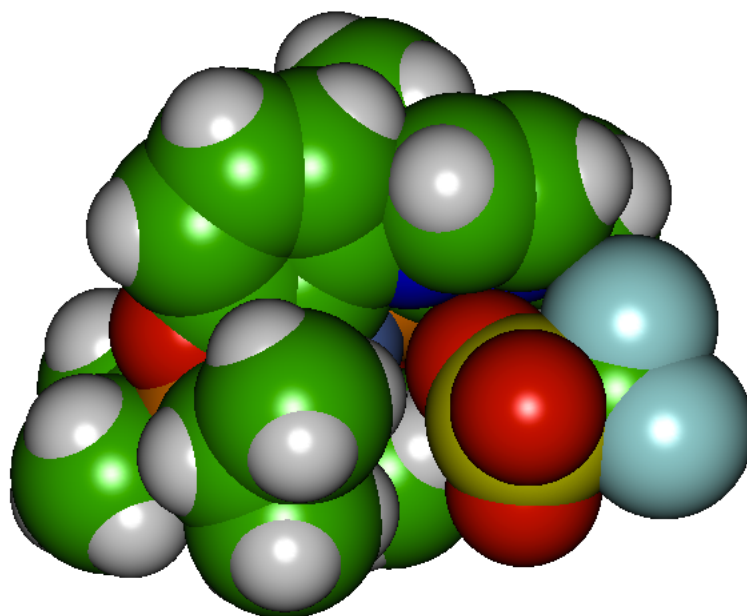


Figure S3. Space filling model of complex $[4]^+$.

Calc. PCM-B3PW91/6-31G** Ni-OTf : 2.522 Å et N ₂ C-OTf : 3.024 Å Ni _{5c} -N(CCH ₃): 1.853 Å	Exp. (DRX) Ni-OTf : 2.433 Å et N ₂ C-OTf : 3.074 Å Ni _{5c} -N(CCH ₃): 1.894 Å
PBE-D3/6-31G** Ni-OTf : 2.250 Å et N ₂ C-OTf : 2.804 Å Ni _{5c} -N(CCH ₃): 1.842 Å	M06/6-31G** Ni-OTf : 2.298 Å et N ₂ C-OTf : 2.774 Å Ni _{5c} -N(CCH ₃): 1.874 Å
PCM-M06L/Def2TZVP Ni-OTf : 2.484 Å et N ₂ C-OTf : 2.926 Å Ni _{5c} -N(CCH ₃): 1.893 Å	PCM-M06/6-31G** Ni-OTf : 2.420 Å et N ₂ C-OTf : 2.873 Å Ni _{5c} -N(CCH ₃): 1.861 Å
PCM-M06L/6-311++G(d,p) Ni-OTf : 2.453 Å et N ₂ C-OTf : 2.901 Å Ni _{5c} -N(CCH ₃): 1.900 Å	PCM-M06L/6-31G**/6-311+G(d)(Ni) Ni-OTf : 2.403 Å et N ₂ C-OTf : 2.874 Å Ni _{5c} -N(CCH ₃): 1.894 Å
PCM-M11/Def2TZVP/ Def2TZVPD(Ni) Ni-OTf : 2.515 Å et N ₂ C-OTf : 2.903 Å Ni _{5c} -N(CCH ₃): 1.938 Å	

Figure S4. Selected geometrical data for the ⁱPrPIMIOCOPⁱPr pincer-type Ni complex **1** calculated at various levels in the gas phase or in acetonitrile solvent using the polarizable continuum model (PCM).

Table S1. Sensitivity to the basis set of the ELF analysis of experimental geometry of **1**. B3PW91 level of calculation. a: Populations of ELF basins in e^- . b: Angles in degrees.

	6-31G**	6-31++G**	DGDZVP	cc-pVDZ	AUG-cc-pVDZ	Def2SVP	Def2SVPP	Def2TZVP
V(Ni) ^a	0.29	0.38	0.77	0.15	1.27	1.19	1.15	-
C(Ni) ^a	25.79	25.58	25.40	25.83	24.84	25.14	25.17	25.81
ELF	0.311	0.282	0.292	0.000	0.266	0.265	0.266	-
V(Ni)-Ni (Å)	1.102	1.091	0.992	V(Asyn)		-	-	-
V(Ni)-C(Ni)-V(Ni.P) ^b	75.9	78.3	69.8	-		-	-	-
	88.5	84.8	88.3	-		-	-	-
Volume V(Ni) (bohr ³)	14.37	17.21	17.54	9.69	22.30	22.41	21.94	-

Table S2. ELF analysis of complexes **1-3**. Experimental geometry and B3PW91/6-31G** level of calculation.

	V(Ni,C) ^a	%Ni ^b	Cov. ^c	Dist ^d	V(Ni,PO) ^a V(Ni,P) ^a	%Ni ^b	Cov. ^c	Dist. ^d	V(N _{CH3CN}) ^a V(O _{H2O}) ^a	%Ni ^b	Cov. ^c	Dist ^d
[1] ⁺	2.14	0.35 16%	-0.36	1.247	2.15 2.15	0.44 0.33	-0.38 -0.30	1.367 1.406	3.18	0.14 4.4 %	-0.22	1.302
[2] ⁺	2.15	0.35 16%	-0.35	1.258	2.13 2.11	0.41 0.32	-0.38 -0.30	1.355 1.401	3.19	0.15 4.4 %	-0.22	1.301
[3] ⁺	2.28	0.38 17%	-0.33	1.258	2.08 2.01	0.40 0.30	-0.29 -0.22	1.324 1.363	1.93 2.32	3.6 % 0.02 0.8 %	-0.08 -0.03	1.378 2.093
OTf	V(O) ^a	%Ni ^b	Cov. ^c	Dist ^e	V(O) ^a	%Ni ^a	Cov. ^d	Dist. ^d	V(Ni) ^a	ELF	Cov. ^b	Dist ^c
[1] ⁺	2.64	0.02	-0.03	0.569	3.43	0.01	-0.03	0.570	0.29	0.311	-0.17	1.102
[2] ⁺	2.33	0.02	-0.03	0.568	3.76	0.01	-0.03	0.568	0.34	0.313	-0.20	1.102
[3] ⁺	2.18	0.0	-0.00	0.573	3.86	0.0	-0.00	0.572	1.58	0.261	-1.04	1.023

^a: Average populations \bar{N} in e ^b: QTAIM atomic contribution of Ni (e). ^c: covariance $\langle \bar{\sigma}^2(V(\text{Ni},X),C(\text{Ni})) \rangle$. ^d: Distance in Å to C(Ni). ^e: Distance in Å to C(O).

Table S3. QTAIM descriptors (in a.u.) of selected bond critical points (BCP) involving the nickel atom or the oxygen atom of the triflate counter-anion interacting with nickel in [1]⁺.

#BCP	BCP	ρ_{bcp}	$\Delta\rho_{\text{bcp}}$	V_{bcp}	H_{bcp}	$ H_{\text{bcp}} /\rho_{\text{bcp}}$	$ V_{\text{bcp}} /G_{\text{bcp}}$	DI	E_{int} (kcal/mol)
10	Ni-C	0.1265	+0.192	-0.177791	-0.064918	0.51	1.58	0.819	55.8
42	Ni-PO	0.1094	+0.077	-0.142833	-0.061737	0.56	1.76	0.763	44.8
57	Ni-P	0.0910	+0.106	-0.118567	-0.046073	0.51	1.64	0.660	37.2
19	Ni-NC	0.1008	+0.559	-0.188894	-0.024622	0.24	1.15	0.570	59.3
82	O-Ni	0.0284	+0.118	-0.031824	-0.001167	0.04	1.04	0.166	10.0
87	O---H	0.0039	+0.016	-0.002178	+0.000699	0.23	0.70	0.013	0.7
4	O---N	0.0088	+0.030	-0.006151	+0.000922	0.08	0.90	0.035	1.9

See BCP labelling in Figure 6 of the manuscript. B3PW91/6-31G** level of calculation.

Table S4. QTAIM characteristics (in a.u.) of selected bond critical points (BCP) involving the nickel atom.

BCP	DI	ρ_{bcp}	$\Delta\rho_{\text{bcp}}$	V_{bcp}	H_{bcp}	$ H_{\text{bcp}} /\rho_{\text{bcp}}$	$ V_{\text{bcp}} /G_{\text{bcp}}$	E_{int} (kcal/mol)
3 Ni-OH ₂	0.462	0.0823	+0.504	-0.148675	-0.011353	0.14	1.08	46.6
2 Ni-NC	0.570	0.1015	+0.567	-0.191115	-0.024717	0.24	1.15	60.0
1 Ni-NC	0.570	0.1008	+0.559	0.188894	-0.024622	0.24	1.15	59.3
1 Ni-OTf	0.166	0.0284	+0.118	-0.031824	-0.001167	0.04	1.04	10.0
2 Ni-OTf	0.186	0.0330	+0.143	-0.040063	-0.002186	0.07	1.06	12.6
3 H-OTf	0.101	0.0426	+0.128	-0.032073	-0.000010	0.00023	1.00	10.1

B3PW91/6-31G** level of calculation.

Table S5. Selected data of ELF analysis performed at the B3PW91/6-31G**//PCM-B3PW91/6-31G**.

	[6] ⁺	[5] ⁺
V(O)	6.12	6.32
QTAIM (Ni)	0.06	0.10
$\langle \bar{\sigma}^2(\text{V(O),C(Ni)}) \rangle$	-0.09	-0.13
V(O)-O (Å)	0.572	0.570
$\delta(\text{O,Ni})$	-0.14	-0.20
V(Ni)	0.30	0.27
C(Ni)	25.75	25.71
ELF	0.314	0.309
V(Ni)-Ni (Å)	1.131	1.167
V(Ni)-C(Ni)-V(Ni.P)	81.3°	84.6°
Angles in degrees	65.7°	80.1°
Volume of V(Ni) (bohr ³)	14.37	13.51

Table S6. QTAIM characteristics (^a in a.u.) of the Ni-O bond critical points (BCP) related to the interaction of the nickel atom with the oxygen atom of the counter-anion. B3PW91/6-31G**//PCM-B3PW91/6-31G** level of calculation. ^a: Experimental geometry and B3PW91/6-31G** level of calculation.

	BCP	DI	ρ_{bcp}	$\Delta\rho_{\text{bcp}}$	V_{bcp}	H_{bcp}	$ H_{\text{bcp}} /\rho_{\text{bcp}}$	$ V_{\text{bcp}}/G_{\text{bcp}} $	E_{int} (kcal/mol)
[1] ⁺ ^a	Ni-OTf	0.166	0.0284	+0.118	-0.031824	-0.001167	0.04	1.04	10.0
[6] ⁺	Ni-OP	0.272	0.0462	+0.172	0.061565	-0.009231	0.20	1.18	19.3
[5] ⁺	Ni-OSi	0.392	0.0668	+0.250	-0.099403	-0.018384	0.28	1.22	31.2

Table S7. Selected data of ELF analysis performed at the B3PW91/6-31G**//PCM-B3PW91/6-31G**.

	[1] ⁺ ^a	[8] ⁺⁺ C ₁	7
V(O)	2.64	6.08	0.84
	3.43		2.94
			2.33
QTAIM (Ni)	0.02	0.08	0.04
	0.01		0.02
			0.02
< $\bar{\sigma}^2(\text{V(O),C(Ni)})$ >	-0.03	-0.10	-0.04
	-0.03		-0.03
			-0.03
			0.570 (1.389)
V(O)-O (V(O)-Ni) (Å)	0.569	0.569 (2.343)	0.569 (2.190)
			0.566 (2.127)
$\delta(\text{O,Ni})$	-0.08	-0.20	-0.23
V(Ni)	0.29	1.83 ^b	1.64
C(Ni)	25.79	24.69	24.57
ELF	0.311	0.237	0.239
V(Ni)-Ni (Å)	1.102	1.045	-
V(Ni)-C(Ni)-V(Ni.P)	75.9°	71.8	-
Angles in degrees	88.5°	158.3	-
Volume of V(Ni) (bohr ³)	14.37	29.44	25.37

^a: Experimental geometry and B3PW91/6-31G** level of calculation.

Table S8. QTAIM characteristics (^a in a.u.) of the Ni-O bond critical points (BCP) related to the interaction of the nickel atom with the oxygen atom of the triflate counter-anion.

Pincer	DI	ρ_{bcp}	$\Delta\rho_{\text{bcp}}$	V_{bcp}	H_{bcp}	$ H_{\text{bcp}} /\rho_{\text{bcp}}$	$ V_{\text{bcp}}/G_{\text{bcp}} $	E_{int} (kcal/mol)
[1] ⁺ ^a	0.166	0.0284	+0.118	-0.031824	-0.001167	0.040	1.04	10.0
[8] ⁺⁺	0.39	0.071	+0.304	-0.112	-0.018	0.254	1.19	35.1
7	0.45	0.078	0.464	-0.139	-0.012	0.154	1.09	43.6

B3PW91/6-31G**//PCM-B3PW91/6-31G** level of calculation. ^a: Experimental geometry and B3PW91/6-31G** level of calculation.

Table S9. Selected data of ELF analysis performed at the B3PW91/6-31G**//PCM-B3PW91/6-31G**.

	[1] ⁺ ^a	[9] ⁺	[10] ⁺	[12] ⁺
V(O)	2.64 3.43	3.71 2.48	6.17	6.20
QTAIM (Ni)	0.02 0.01	0.02 0.03	0.05	0.10
< $\bar{\sigma}^2(V(O),C(Ni))$ >	-0.03 -0.03	-0.04 -0.04	-0.09	-0.13
V(O)-O (Å)	0.569	0.568 0.566	0.567	0.570
$\delta(O,Ni)$	-0.08	-0.13	-0.13	-0.20
V(Ni)	0.29	0.30	0.32	1.12
C(Ni)	25.79	25.62	25.63	24.71
ELF	0.311	0.305	0.307	0.258
V(Ni)-Ni (Å)	1.102	1.099	1.091	na
V(Ni)-C(Ni)-V(Ni.P)	75.9°	73.0	85.0	-
Angles in degrees	88.5°	-	85.6	-
Volume of V(Ni) (bohr ³)	14.37	13.34	13.07	15.92

^a: Experimental geometry and B3PW91/6-31G** level of calculation.

Table S10. QTAIM characteristics (in a.u.) of the Ni-O bond critical points (BCP) related to the interaction of the nickel atom with the oxygen atom of the triflate counter-anion.

	L	DI	ρ_{bcp}	$\Delta\rho_{bcp}$	V_{bcp}	H_{bcp}	$ H_{bcp} /\rho_{bcp}$	$ V_{bcp}/G_{bcp} $	E_{int} (kcal/mol)
[1] ⁺ ^a	CH3CN	0.166	0.0284	+0.118	-0.031824	-0.001167	0.04	1.04	10.0
[9] ⁺	CO	0.26	0.044	0.167	-0.058	-0.008	0.181	1.16	18.2
[10] ⁺	CO	0.26	0.046	0.180	-0.062	-0.009	0.196	1.15	19.5
[12] ⁺	NO ⁺	0.39	0.070	0.270	-0.106	-0.019	0.271	1.22	33.3

B3PW91/6-31G**//PCM-B3PW91/6-31G** level of calculation. ^a: Experimental geometry and B3PW91/6-31G** level of calculation.

Crystal Structure Determinations of **1**, **2** and **3**.

The crystallographic data for **1**, **2** and **3** were collected on a Bruker APEX II equipped with an Incoatec I μ S Microsource and a Quazar MX monochromator. Cell refinement and data reduction were done using SAINT.¹ An empirical absorption correction, based on the multiple measurements of equivalent reflections, was applied using the program SADABS.² The space group was confirmed in each case by XPREP routine³ in the program SHELXTL.⁴ The structures were solved by direct methods and refined by full matrix least-squares and difference Fourier techniques with SHELX-97.⁵ All non-hydrogen atoms were refined with anisotropic displacement parameters. Hydrogen atoms were set in calculated positions and refined as riding atoms with a common thermal parameter. Complete details of the X-ray analyses reported herein have been deposited at The Cambridge Crystallographic Data Centre (CCDC 1519756 (**1**), 1519757 (**2**), 1519755 (**3**)). This data can be obtained free of charge via [www.ccdc.cam.ac.uk/ data_request/cif](http://www.ccdc.cam.ac.uk/data_request/cif), or by emailing data_request@ccdc.cam.ac.uk, or by contacting The Cambridge Crystallographic Data Centre, 12, Union Road, Cambridge CB2 1EZ, U.K.; fax: +44 1223 336033.

Table S11. Crystallographic information for complexes **1**, **2** and **3**.

	[(i-Pr-PIMIOCOP)Ni-(NCCH ₃)] ₂ [OTf] ₂ 1	[(Ph-PIMIOCOP)Ni-(NCCH ₃)] ₂ [OTf] ₂ 2	[(i-Pr-PIMIOCOP)Ni-(OH ₂)] ₂ [OTf] ₂ 3
chemical formula	C ₂₅ H ₃₉ F ₃ N ₃ NiO ₄ P ₂ S, CF ₃ O ₃ S,CHCl ₃	C ₃₇ H ₃₁ F ₃ N ₃ NiO ₄ P ₂ S, CF ₃ O ₃ S, CHCl ₃	C ₂₂ H ₃₈ N ₂ NiO ₂ P ₂ , C ₄ H ₈ O ₂ ,2(CF ₃ O ₃ S)
Crystal color	yellow	yellow	yellow
<i>F</i>_w; <i>F</i>(000)	923.74; 474	1059.80; 1076	853.44; 1776
<i>T</i> (K)	100	100	100
wavelength (Å)	1.54178	1.54178	1.54178
space group	P1	P-1	P212121
<i>a</i> (Å)	8.6387(1)	11.5371(2)	12.6237(2)
<i>b</i> (Å)	10.2452(1)	13.0220(2)	14.7496(3)
<i>c</i> (Å)	12.3646(2)	15.8726(2)	20.0982(4)
α (deg)	110.392(1)	70.9497(8)	90.00
β (deg)	96.636(1)	78.8376(9)	90.00
γ (deg)	106.480(1)	79.3474(8)	90.00
<i>Z</i>	1	2	4
<i>V</i> (Å³)	955.22(2)	2192.29(6)	3742.18(12)
ρ_{calc} (g·cm⁻³)	1.606	1.605	1.515
μ (mm⁻¹)	5.158	4.593	3.322
θ range (deg); completeness	3.927 – 71.013; 0.974	2.98 – 71.10; 0.964	3.72 – 71.19; 0.999
collected reflections; <i>R</i>_{σ}	25147; 0.0243	43338; 0.0300	95894; 0.0159
unique reflections; <i>R</i>_{int}	25147; 0.022	43338; 0.043	95894; 0.040
<i>R</i>1^a; w<i>R</i>2^b [<i>I</i> > 2σ(<i>I</i>)]	0.0220; 0.0554	0.0451; 0.1232	0.0345; 0.1090
<i>R</i>1; w<i>R</i>2 [all data]	0.0221; 0.0554	0.0519; 0.1297	0.0350; 0.1097
GOF	1.048	1.038	1.047
largest diff peak and hole	0.346 and -0.238	1.321 and -0.686	0.867 and -0.407
CIF number	CCDC 1519756	CCDC 1519757	CCDC 1519755

References.

¹ SAINT, Release 6.06; Integration Software for Single Crystal Data; Bruker AXS Inc.: Madison, WI, 1999.

² Sheldrick, G. M. SADABS, Bruker Area Detector Absorption Corrections; Bruker AXS Inc., Madison, WI, 1999.

³ XPREP, Release 5.10; X-ray Data Preparation and Reciprocal Space Exploration Program; Bruker AXS Inc.: Madison, WI, 1997.

⁴ SHELXTL, Release 5.10; The Complete Software Package for Single Crystal Structure Determination; Bruker AXS Inc.: Madison, WI, 1997.

⁵ (a) Sheldrick, G. M. SHELXS97, Program for the Solution of Crystal Structures; Univ. of Gottingen: Germany, 1997. (b) Sheldrick, G. M. SHELXL97, Program for the Refinement of Crystal Structures; University of Gottingen: Germany, 1997.